Elliptic and triangular flow of charmonium states in heavy ion collisions

Sungtae Cho
Division of Science Education, Kangwon National University, Chuncheon 24341, Korea

(Received 3 August 2023; revised 22 February 2024; accepted 27 March 2024; published 6 May 2024)

I study the elliptic and triangular flow of charmonium states, or J/ψ, $\psi(2S)$, and $\chi_c(1P)$ mesons in heavy ion collisions. Starting from the evaluation of charmonia transverse momentum distributions and yields, I calculate elliptic and triangular flow of charmonium states based on the coalescence model. I show that the internal structure, or the wave function distribution of charmonium states plays a significant role, especially when charmonium states are produced by charm quark recombination, leading to the transverse momentum distribution of the $\psi(2S)$ meson as half large as that of the J/ψ meson. I also consider the dependence of the elliptic and triangular flow of charmonium states on internal structures of charmonium states, and find that the wave function effects as well as feed-down contributions are averaged out for elliptic and triangular flow, resulting in similar elliptic and triangular flow for all charmonium states. I investigate further the elliptic and triangular flow of charmonium states at low transverse momentum region, and also discuss the quark number scaling of elliptic and triangular flow for charmonium states.

DOI: 10.1103/PhysRevC.109.054904

I. INTRODUCTION

It has been expected that a new form of the matter composed of deconfined partonic states, the so-called quark-gluon plasma (QGP), is created in the environments of high temperatures enough to set quarks and gluons free from hadrons [1]. Since the QGP disappears very quickly and is converted into hadrons in a time scale of strong interactions, various ways of recognizing the existence of the QGP or the phase transition to the QGP in heavy ion collisions have been sought out. As one of the plausible tools for the probe of the QGP, a heavy quarkonium, i.e., the J/ψ meson has been proposed from the expectation that the production of the J/ψ is suppressed in the QGP medium due to the dissociation of the J/ψ by the Debye color screening between charm and anticharm quarks [2].

With much larger achievable energy than ever before possible in experiments carried out at the Large Hadron Collider (LHC), other charmonium states, as well as the J/ψ meson, are estimated to be more abundantly produced, thereby becoming convenient probes and presenting us with important information on many properties of the QGP [3–5]. These charmonium states are expected to play significant roles as probes to the temperature variation of the QGP during the time evolution in heavy ion collisions since they dissociate in the QGP at different temperatures depending on the strength of their binding energies [6–8].

The effects of the quark-gluon plasma on the J/ψ meson are mostly observed with the ratio between the yield of the J/ψ in heavy ion collisions and that in $p+p$ collisions rescaled by the number of binary collisions, i.e., the so-called nuclear modification factor, R_{AA}. In the early measurement at the Relativistic Heavy Ion Collider (RHIC), the R_{AA} of the J/ψ decreases with the number of participating nucleons or with increasing centralities, implying that the J/ψ production is actually suppressed due to the presence of the QGP and is more suppressed with increasing size of the QGP [9].

On the other hand, the same measurement on the R_{AA} of the J/ψ in collision energies ten times larger at LHC by ALICE Collaboration shows that the R_{AA} of J/ψ mesons is not dependent on centralities anymore, meaning the less suppression of the J/ψ production at the QGP and supporting possibilities of the J/ψ regeneration from charm quarks in the QGP [10,11]. Especially, the enhancement of the R_{AA} of the J/ψ observed at low transverse momentum region [11] strongly favors the scenario that the significant amount of the J/ψ meson is produced from a charm and an anticharm quarks by recombination in the QGP.

Recent measurements by ALICE Collaboration show that the R_{AA} of the $\psi(2S)$ meson is also independent of centralities as that of the J/ψ, indicating that the significant amount of $\psi(2S)$ mesons are regenerated as well from charm quarks in the QGP [12]. Compared to the R_{AA} of the J/ψ, however, the R_{AA} of the $\psi(2S)$ meson is half as large as that of the J/ψ, raising the possibility of the different production mechanism between the J/ψ and $\psi(2S)$ when they are produced by charm quark recombination from the QGP.

Moreover, the measurement by CMS Collaboration on the nuclear modification factor ratio between the $\psi(2S)$ and J/ψ in the transverse momentum p_T and rapidity y ranges, $3 < p_T < 30$ GeV and $1.6 < |y| < 2.4$ at $\sqrt{s_{\rm NN}} = 2.76$ TeV shows that the ratio increases with an increasing number of participants or with increasing centralities [13]. The similar measurement in different transverse momentum and rapidity regions, $9 < p_T < 40$ GeV and $|y| < 2$ by ATLAS Collaboration at $\sqrt{s_{\rm NN}} = 5.02$ TeV also shows that the prompt $\psi(2S)$ to J/ψ double ratio increases with increasing number of participants [14], implying that different amounts of the

J/ψ and $\psi(2S)$ are produced when they are affected by the QGP in heavy ion collisions.

It has been known that the yield in the coalescence production is dependent on the overlap between the Wigner distribution or the coalescence probability function, which is made up of the wave function of the produced hadron, and the phase space density functions or the transverse momentum distributions of constituents [15–18]. Reminding that both the J/ψ and $\psi(2S)$ share the charm and anticharm quarks as their constituents, one may confirm different coalescence probabilities for the cause of different amounts of the J/ψ and $\psi(2S)$ yields when the J/ψ and $\psi(2S)$ are formed from the same source in the QGP by recombination.

The investigation on the production of not only the J/ψ meson but also $\psi(2S)$ and $\chi_{c1}(1P)$ mesons from the QGP by recombination has already been made [19]. The study has shown that when these charmonia are produced by charm quark coalescence, the $\psi(2S)$ meson can be produced half as much as the J/ψ meson, which is a substantial enhancement in the production of the $\psi(2S)$ compared to that of the J/ψ, especially considering the mass difference of about 600 MeV between these two charmonium states. The enhanced production of the $\psi(2S)$, or the different amount of yields for different charmonium states has been found to originate from the different amounts of overlap between the different Wigner functions for each charmonium state and the same distribution of constituents in phase space, in other words, the different amounts of overlap between different wave function distributions from different internal structures, $1S$, $2S$, and $1P$ of charmonia and the same transverse momentum distribution of charm quarks in momentum space [19].

In addition to the transverse momentum distribution of charmonium states, the elliptic flow of charmonium states is also dependent on their wave function distributions through the coalescence probability function; the elliptic flow of hadrons is known to bear the elliptic flow of constituents caused by their anisotropic configurations at the moment of heavy ion collisions when hadrons are produced by quark coalescence [20]. Since the elliptic flow of hadrons is dependent on transverse momentum distributions of constituents, to be exact, the transverse momentum distribution anisotropy of quarks via the transverse momentum distribution of hadrons, the elliptic flow of charmonium states are also expected to be dependent on their internal structures, thereby giving rise to different elliptic flows for different charmonium states when charmonium states of different internal structures are produced from charm quarks by recombination.

The study on the elliptic flow of charmonium states has already been carried out experimentally, e.g., Ref. [21], but the consideration of different coalescence probability functions for different charmonium states has been overlooked. Moreover, it has not been investigated whether or not the so-called quark number scaling of hadrons, which states that the elliptic flow of hadrons is similar in size to the elliptic flow of a quark times the number of quarks inside hadrons [20], is also applicable to the elliptic flow of charmonium states when charmonium states with different internal structures are produced from the same number of charm quarks by coalescence.

Therefore, it is necessary to reevaluate the elliptic flow of each charmonium state produced from charm quarks by coalescence in heavy ion collisions in order to investigate the dependence of the elliptic flow of charmonium states on their wave function distribution in momentum space as well as the applicability of the quark number scaling of elliptic flow to the case of charmonium states. This study may help us to understand the recent observation by CMS Collaboration on the transverse momentum distribution of the elliptic flow of not only the J/ψ but also the $\psi(2S)$ [22], showing different transverse momentum distributions of the elliptic flow between the J/ψ and $\psi(2S)$.

In addition, the CMS Collaboration also reported the observation of the triangular flow of the J/ψ in heavy ion collisions [22]. In line with this observation, I find it is also necessary to study the triangular flow of charmonium states when charmonium states of different internal structures are produced from the same charm quark triangular flow by coalescence, and therefore, I extend the discussion on the elliptic flow of charmonium states to the study on the higher flow harmonics of charmonium states as well.

As is well known, the flow harmonics, such as the elliptic and triangular flow, originate from the initial geometry of nucleus at the moment of heavy ion collisions; the pressure gradient generated in the particular shape caused by the anisotropic initial collisions creates various kinds of flows or flow harmonics. In addition to the anisotropy of nucleon distributions in heavy ion collisions, event-by-event fluctuations in heavy ion collisions are also found to be important origins, especially giving rise to higher flow harmonics, e.g., the triangular flow [23–27]. I discuss here mainly the contribution of the triangular flow of charmonium states built from the triangular flow of charm quarks due to the initial anisotropic heavy ion collisions in the same way that the elliptic flow of charmonium states are formed from that of charm quarks by recombination.

The paper is organized as follows. In Sec. II, I discuss transverse momentum distributions and yields of charmonium states, the J/ψ, $\psi(2S)$, and $\chi_{c1}(1P)$. I investigate the different internal structures of charmonium states, and calculate their yields and transverse momentum distributions, which are dependent on their internal structures or their wave function distributions in momentum space. In Sec. III, I evaluate elliptic and triangular flow of charmonium states when they are produced from charm quark elliptic and triangular flow by recombination at the quark-hadron phase boundary. I further show the quark number scaling of elliptic and triangular flow for charmonium states, and also present comparison between the present evaluation and various experimental measurements in Sec. III. I discuss the dependence of transverse momentum distributions, yields, and flow harmonics of charmonium states on their internal structure, or the wave function distribution of each charmonium state in momentum space in Sec. IV. Finally, I present a summary and conclusion in Sec. V.

II. TRANSVERSE MOMENTUM DISTRIBUTIONS AND YIELDS OF CHARMONIUM STATES

I first consider the meson produced from the quark-gluon plasma by quark coalescence. When a meson is formed from

a quark, q and an antiquark, $\bar{q}$, the yield of the meson in the coalescence model is described by [16],

$$N = g \int p_q \cdot d\sigma_q p_{\bar{q}} \cdot d\sigma_{\bar{q}} \frac{d^3\vec{p}_q}{(2\pi)^3 E_q} \frac{d^3\vec{p}_{\bar{q}}}{(2\pi)^3 E_{\bar{q}}} \times f_q(r_q, p_q) f_{\bar{q}'}(r_{\bar{q}'}, p_{\bar{q}}) W(r_q, r_{\bar{q}}; p_q, p_{\bar{q}}), \quad (1)$$

where $d\sigma$ is a hypersurface element, and $f_q(r, p)$ and $f_{\bar{q}}(r, p)$ are, respectively, covariant distribution functions of a quark and an antiquark satisfying the following normalization condition,

$$\int p \cdot d\sigma \frac{d^3\vec{p}_{q(\bar{q})}}{(2\pi)^3 E_{q(\bar{q})}} f_{q(\bar{q})}(r, p) = N_{q(\bar{q})}, \quad (2)$$

the number of all (anti)quarks available in the system. The factor g takes into account the chance of generating a meson from quarks, e.g., $g_{J/\psi} = 3/(2 \times 3)^2$. In Eq. (1), $W(r_q, r_{\bar{q}}; p_q, p_{\bar{q}})$ is the coalescence probability function, or the so-called Wigner function made up of wave functions of the hadron produced by coalescence.

Under the assumption of boost-invariant longitudinal momentum distributions of (anti)quarks satisfying $\eta = y$, or the Bjorken correlation between spatial and momentum rapidities, the transverse momentum distribution of the yield for the meson can be derived in the nonrelativistic limit from Eq. (1) into [15,16,28,29],

$$\frac{d^2N}{dp_T^2} = \frac{g}{V} \int d^3\vec{r} d^2\vec{p}_{qT} d^2\vec{p}_{\bar{q}T} \delta^{(2)}(\vec{p}_T - \vec{p}_{qT} - \vec{p}_{\bar{q}T}) \times \frac{d^2N_q}{dp_{qT}^2} \frac{d^2N_{\bar{q}}}{dp_{\bar{q}T}^2} W(\vec{r}, \vec{k}), \quad (3)$$

where $d^2N_{q(\bar{q})}/d^2\vec{p}_{q(\bar{q})T}$ is the number of (anti-) quarks as a function of transverse momentum, and $W(\vec{r}, \vec{k})$ is the Wigner function,

$$W(\vec{r}, \vec{k}) = \int \frac{d^3\vec{q}}{(2\pi)^3} \tilde{\psi}^*\left(\vec{k} + \frac{\vec{q}}{2}\right) e^{-i\vec{r}\cdot\vec{q}} \tilde{\psi}\left(\vec{k} - \frac{\vec{q}}{2}\right), \quad (4)$$

with $\vec{r}$ and $\vec{k}$ being, respectively, the distance and relative momentum between a quark and an antiquark in a meson rest frame. The Wigner function has been normalized on the condition, $\int W(\vec{r}, \vec{k}) d^3\vec{r} d^3\vec{k} = (2\pi)^3$, and the $\tilde{\psi}(\vec{k})$ in Eq. (4) is the wave function of the meson produced by quark coalescence in momentum representation.

In the same manner, the transverse momentum distribution of charmonium states can be derived as represented in Eq. (3),

$$\frac{d^2N_M}{dp_T^2} = \frac{g_M}{V} \int d^3\vec{r} d^2\vec{p}_{cT} d^2\vec{p}_{\bar{c}T} \delta^{(2)}(\vec{p}_T - \vec{p}_{cT} - \vec{p}_{\bar{c}T}) \times \frac{d^2N_q}{dp_{cT}^2} \frac{d^2N_{\bar{c}}}{dp_{\bar{c}T}^2} W_M(\vec{r}, \vec{k}), \quad (5)$$

where subscript M in Eq. (5) stands for the kind of charmonium states, e.g., s for J/ψ, p for $\chi_{c1}(1P)$, and 10 for $\psi(2S)$.

As shown in Eq. (5), yields or transverse momentum distributions of charmonium states produced by quark coalescence are mainly dependent on two factors, the transverse momentum distribution of charm quarks and the Wigner function. Reminding that all different charmonium states, the J/ψ, $\chi_c(1P)$, and $\psi(2S)$ have the same charm quark components, one can expect that the Wigner function plays a major role in Eq. (5) in characterizing the production of different charmonium states from the same charm quark constituents by charm quark coalescence, as already pointed out in Ref. [19].

As the Wigner function is constructed from the wave function of hadron produced by coalescence, Eq. (4), the transverse momentum distribution, and also the yield of charmonium states should be dependent on the wave function of charmonium states through the Wigner function, e.g., the Wigner function of the J/ψ must be different from that of the $\psi(2S)$; the J/ψ meson is an s-wave state whereas the $\psi(2S)$ is a radially excited state of the J/ψ. It should be noted that the internal structure of the $\chi_c(1P)$ meson is also different from those of the J/ψ and $\psi(2S)$ meson; the $\chi_c(1P)$ meson is in a p-wave state.

One can investigate the explicit dependence of the transverse momentum distribution of charmonium states on the wave function by considering various types of wave functions. In general, Gaussian-type wave functions are chosen for the description of the wave function of hadrons. On the other hand, one can also consider Coulomb-type wave functions, especially for charmonium states. Since charmonium states can be considered as the charm and anticharm quark bound state formed by a color Coulomb interaction between charm and anticharm quarks [2], as an analogue of the electromagnetic Coulomb interaction between an electron and a proton inside a hydrogen atom, the Coulomb wave function can also be adopted in describing the wave function of charmonium states.

The explicit representation of the Wigner function constructed from Coulomb wave functions for charmonium states as well as the dependence of the transverse momentum distribution of charmonium states on both Coulomb and Gaussian wave functions have already been discussed [19]. It has been shown that transverse momentum distributions of the J/ψ and $\psi(2S)$ meson are clearly dependent on their wave functions, and also the detailed comparison between transverse momentum distribution of the J/ψ and $\psi(2S)$ based on both Coulomb and Gaussian wave functions has been made [19].

With this in mind, I apply in this work different wave functions, or different Wigner functions for different charmonium states in evaluating both yield distributions as functions of transverse momenta and flow harmonics such as v_2 and v_3 as an attempt to investigate differences in the production of different charmonium states. However, I do not adopt here both types of wave functions, the Coulomb and Gaussian, and confine the discussion on the results only obtained with Gaussian-type wave functions so as to focus, without loss of generality, on differences between charmonium states in their production by charm quark coalescence at the quark-hadron phase boundary.

The Wigner functions based on Gaussian wave functions have already been obtained for s-, p- [30,31] and d-wave [32]

states,

$$W_s(\vec{r},\vec{k}) = 8e^{-\frac{r^2}{\sigma^2}-k^2\sigma^2}$$
$$W_p(\vec{r},\vec{k}) = \left(\frac{16}{3}\frac{r^2}{\sigma^2} - 8 + \frac{16}{3}\sigma^2k^2\right)e^{-\frac{r^2}{\sigma^2}-k^2\sigma^2}$$
$$W_d(\vec{r},\vec{k}) = \frac{8}{15}\left(4\frac{r^4}{\sigma^4} - 20\frac{r^2}{\sigma^2} + 15 - 20\sigma^2k^2 + 4\sigma^4k^4 + 16r^2k^2 - 8(\vec{r}\cdot\vec{k})^2\right)e^{-\frac{r^2}{\sigma^2}-k^2\sigma^2}, \quad (6)$$

where an oscillator frequency ω is related to the reduced mass μ with $\sigma^2 = 1/(\mu\omega)$. The $2S$ state Wigner function based on a Gaussian wave function is also available [19],

$$W_{10}(\vec{r},\vec{k}) = \frac{16}{3}\left(\frac{r^4}{\sigma^4} - 2\frac{r^2}{\sigma^2} + \frac{3}{2} - 2\sigma^2k^2 + \sigma^4k^4 - 2r^2k^2 + 4(\vec{r}\cdot\vec{k})^2\right)e^{-\frac{r^2}{\sigma^2}-k^2\sigma^2}, \quad (7)$$

constructed from three-dimensional harmonic oscillator wave functions. The subscript 10 represents the first excited state, ψ_{10} from its ground state, ψ_{00} with the lowest angular momentum, describable for the wave function of the $\psi(2S)$ meson. The more Wigner function for higher excited states also constructed from three-dimensional harmonic oscillator wave functions together with phase space distributions have been systematically investigated recently [33].

The Wigner function in Eqs. (6) and (7), can be simplified to the absolute value square of the wave function in momentum representation when it is integrated over coordinate space, $\vec{r}$ with the help of one of important properties of the Wigner function [34],

$$\int d^3\vec{r}W(\vec{r},\vec{k}) = |\tilde{\psi}(\vec{k})|^2. \quad (8)$$

The $\tilde{\psi}(\vec{k})$ is the wave function in momentum representation, corresponding to the coordinate space wave function adopted in the Wigner function $\psi(\vec{r})$.

Applying Eq. (8) to Eq. (3), one can obtain the simpler yield distribution as a function of transverse momentum,

$$\frac{d^2N_M}{dp_T^2} = \frac{g_M}{V}\int d^2\vec{p}_{cT}d^2\vec{p}_{\bar{c}T}\delta^{(2)}(\vec{p}_T - \vec{p}_{cT} - \vec{p}_{\bar{c}T}) \times \frac{d^2N_c}{dp_{cT}^2}\frac{d^2N_{\bar{c}}}{dp_{\bar{c}T}^2}|\tilde{\psi}_M(\vec{k})|^2. \quad (9)$$

The absolute value square of the wave function in momentum representation for each charmonium state is given by,

$$|\tilde{\psi}_M(\vec{k})|^2 = \begin{cases} (2\sqrt{\pi}\sigma)^3e^{-k^2\sigma^2} & \psi_s; J/\psi \\ \frac{2}{3}(2\sqrt{\pi}\sigma)^3e^{-k^2\sigma^2}\sigma^2k^2 & \psi_p; \chi_{c1}(1P) \\ \frac{2}{3}(2\sqrt{\pi}\sigma)^3e^{-k^2\sigma^2}\left(\sigma^2k^2 - \frac{3}{2}\right)^2 & \psi_{10}; \psi(2S). \end{cases} \quad (10)$$

When evaluating the transverse momentum distribution of the charmonium yield, Eq. (9), I only consider the contribution from transverse momenta by neglecting the longitudinal momentum in the wave function at midrapidities $y = 0$ [19,32]; the relative momentum between charm quarks becomes $\vec{k} = (\vec{p}'_{cT} - \vec{p}'_{\bar{c}T})/2$ with $\vec{p}'_{cT}$ and $\vec{p}'_{\bar{c}T}$ being the transverse momenta in the charmonium frame, converted from the transverse momenta of charm and anticharm quarks, $\vec{p}_{cT}$ and $\vec{p}_{\bar{c}T}$ in a fireball frame by the Lorentz transformation [29,35].

In order to evaluate Eq. (9), it is necessary to determine an oscillator frequency, ω, which is related to the size of charmonium states produced by charm quark coalescence [29,36,37]. Here, I adopt oscillator frequencies $\omega = 0.078$ GeV at RHIC and $\omega = 0.076$ GeV at LHC [37] obtained on the condition that all charm quarks at zero transverse momentum are hadronized exclusively by quark coalescence [29,37]. In determining above oscillator frequencies, a total of 14 single charmed hadrons, i.e., ten charm baryons, Λ_c, $\Sigma_c(2455)$, $\Sigma_c(2520)$, $\Lambda_c(2595)$, $\Lambda_c(2625)$, Ξ_c, Ξ'_c, $\Xi_c(2645)$, Ω_c, and $\Omega_c(2770)$, and four open charm mesons, D, D^*, D_s, and D_s^* have been taken into account. Since the yields of charmonium states, made up of charm and anticharm quarks, are much smaller compared to those of single charmed hadrons mentioned above, the oscillator frequencies are found to be almost unchanged as $\omega = 0.078$ GeV at RHIC and $\omega = 0.076$ GeV at LHC even though charmonium states are included in the above calculation of oscillator frequencies on the same condition.

Based on the relation between the mean-square radius, $\langle r^2\rangle$ and the oscillator frequency, $\sigma^2 = 1/(\mu\omega)$ for charmonium states $\langle r^2\rangle_{J/\psi} = 3/2\sigma^2_{J/\psi}$, $\langle r^2\rangle_{\chi_{c1}(1P)} = 5/2\sigma^2_{\chi_{c1}(1P)}$, and $\langle r^2\rangle_{\psi(2S)} = 7/2\sigma^2_{\psi(2S)}$ [19] the size of charmonium states can be evaluated when the above oscillator frequencies are adopted. Using $\omega = 0.078$ or $\omega = 0.076$ GeV one obtains, respectively, 1.0, 1.3, and 1.5 fm for the root-mean-square radii $\sqrt{\langle r^2\rangle}$ of J/ψ, $\chi_{c1}(1P)$, and $\psi(2S)$ states.

In addition to oscillator frequencies, it is also necessary to have the information on the transverse momentum distribution of charm quarks in the system d^2N_c/dp_{cT}^2 in Eq. (9). Here I introduce the following transverse momentum distributions of charm quarks at midrapidity in 0–10 % centrality [38],

$$\frac{d^2N_c^R}{dp_{cT}^2} = \begin{cases} a_0^Re^{(-1.22(p_{cT}/p_{0T})^{1.57})} & p_{cT} \leqslant 1.85\,\text{GeV} \\ a_1^Re^{(-3.04(p_{cT}/p_{0T})^{0.71})} + a_2^R(1.0 + (p_{cT}/p_{0T})^{2.02})^{-3.48} & p_{cT} > 1.85\,\text{GeV} \end{cases}$$
$$\frac{d^2N_c^L}{dp_{cT}^2} = \begin{cases} a_0^Le^{(-0.35(p_{cT}/p_{0T})^{2.47})} & p_{cT} \leqslant 1.85\,\text{GeV} \\ a_1^Le^{(-3.49(p_{cT}/p_{0T})^{3.59})} + a_2^L(1.0 + (p_{cT}/p_{0T})^{0.5})^{-14.31} & p_{cT} > 1.85\,\text{GeV} \end{cases}, \quad (11)$$

TABLE I. Coefficients in the unit of GeV^{-2} in the transverse momentum distributions of charm quarks in the system, d^2N_c/dp_{cT}^2, Eq. (11) at RHIC and LHC, respectively.

	RHIC (GeV^{-2})		LHC (GeV^{-2})
a_0^R	0.69	a_0^L	1.97
a_1^R	1.08	a_1^L	7.95
a_2^R	3.79	a_2^L	87335

with superscripts R and L being represented by a charm quark transverse momentum distribution at RHIC and LHC, respectively. In Eq. (11), $p_{0T} = 1.0$ GeV, and coefficients, a_0^R, a_1^R, a_2^R, a_0^L, a_1^L, and a_2^L are summarized in Table I. The transverse momentum distribution of the charm quark at LHC in Eq. (11) has been obtained for $\sqrt{s_{\rm NN}} = 2.76$ TeV Pb+Pb collisions [38]. The above transverse momentum distributions Eq. (11) corresponds to $dN_c/dy = 2.00$ at RHIC and $dN_c/dy = 14.9$ at LHC for the total number of charm quark pairs, $dN_c/dy = dN_{\bar{c}}/dy$ at a unit midrapidity interval $|y| < 0.5$ in the system [37].

With the transverse momentum distribution of charm quarks Eq. (11) and also the Wigner function Eq. (10) I evaluate transverse momentum distributions of charmonium states J/ψ, $\chi_{c1}(1P)$, and $\psi(2S)$ mesons produced from charm quarks by recombination at the quark-hadron phase transition $d^2N_{J/\psi}/dp_T^2$, $d^2N_{\chi_{c1}(1P)}/dp_T^2$, and $d^2N_{\psi(2S)}/dp_T^2$ at both RHIC $\sqrt{s_{\rm NN}} = 200$ GeV and LHC $\sqrt{s_{\rm NN}} = 2.76$ TeV. I use the coalescence volume 1790 and 3530 fm^3 for RHIC and LHC, respectively, and assume the constituent charm quark mass as 1.5 GeV [37,39].

Shown in Fig. 1 are transverse momentum distributions d^2N/dp_T^2 of charmonium states evaluated at midrapidity in 0–10 % centrality at RHIC $\sqrt{s_{\rm NN}} = 200$ GeV and those multiplied by $2\pi p_T$, dN/dp_T at LHC $\sqrt{s_{\rm NN}} = 2.76$ TeV. Also shown for comparison are experimental measurements of the J/ψ transverse momentum distribution at RHIC $\sqrt{s_{\rm NN}} = 200$ GeV, $|y| < 0.5$ in 0–80 % centrality [40] and the transverse momentum distribution of the J/ψ multiplied by $2\pi p_T$, dN/dp_T measured at LHC $\sqrt{s_{\rm NN}} = 5.02$ TeV, $|y| < 0.9$ in 20–40 % centrality [41]. In evaluating the transverse momentum distributions of J/ψ and $\chi_{c1}(1P)$ as shown in Fig. 1 contributions from the decay of heavier charmonium states are also taken into account, i.e., the significant amount of the J/ψ production comes from other heavier charmonium states, feed downs from $\chi_{c1}(1P)$ and $\psi(2S)$ mesons [42];

$$\frac{d^2N_{J/\psi}^{\rm all}}{dp_T^2} = \frac{d^2N_{J/\psi}}{dp_T^2} + 0.614\,\frac{d^2N_{\psi(2S)}}{dp_T^2} + 0.343\frac{d^2N_{\chi_{c1}}^{\rm all}}{dp_T^2},$$
$$\frac{d^2N_{\chi_{c1}}^{\rm all}}{dp_T^2} = \frac{d^2N_{\chi_{c1}}}{dp_T^2} + 0.0975\,\frac{d^2N_{\psi(2S)}}{dp_T^2}. \qquad (12)$$

I have neglected in Eq. (12) the modification of the transverse momentum distribution of daughter particles from that of a mother particle since decays are mostly radiative, and the mass difference between mother and daughter particles is small compared to the mass of daughter particles.

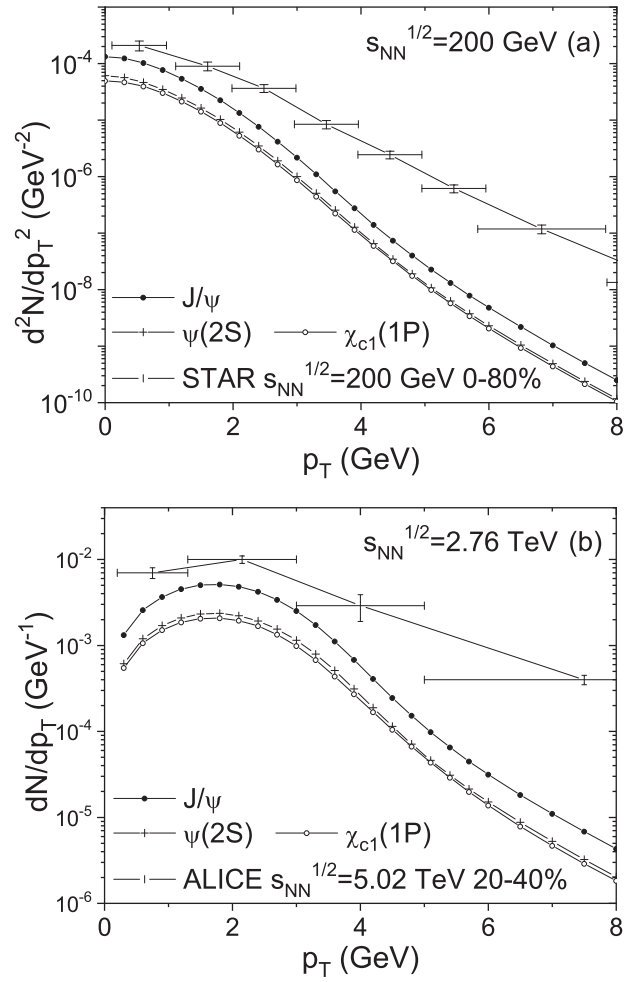

FIG. 1. Transverse momentum distributions d^2N/dp_T^2 of charmonium states at midrapidity in 0–10 % centrality at RHIC $\sqrt{s_{\rm NN}} = 200$ GeV (a) and those multiplied by $2\pi p_T$, dN/dp_T at LHC $\sqrt{s_{\rm NN}} = 2.76$ TeV (b). Also shown for comparison are experimental measurements of (a) the J/ψ transverse momentum distribution at RHIC $\sqrt{s_{\rm NN}} = 200$ GeV [40] at midrapidity in 0–80 % centrality and (b) the transverse momentum distribution of the J/ψ multiplied by $2\pi p_T$, dN/dp_T measured at LHC $\sqrt{s_{\rm NN}} = 5.02$ TeV, $|y| < 0.9$ in 20–40 % centrality [41].

Shown in Fig. 2 are transverse momentum distributions multiplied by $2\pi p_T$, dN/dp_T of charmonium states, J/ψ, $\chi_{c1}(1P)$, and $\psi(2S)$ mesons at midrapidity in 0–10 % centrality when they are purely produced from charm quarks by recombination at the quark-hadron phase transition $d^2N_{J/\psi}/dp_T^2$, $d^2N_{\chi_{c1}}/dp_T^2$ and $d^2N_{\psi(2S)}/dp_T^2$. In addition, shown in the inset of Fig. 2 are the transverse momentum distribution ratios between the $\psi(2S)$ and J/ψ obtained after considering the feed-down contributions following Eq. (12) $d^2N_{\psi(2S)}/dp_T^2/d^2N_{J/\psi}^{\rm all}/dp_T^2$, also at RHIC $\sqrt{s_{\rm NN}} = 200$ GeV and LHC $\sqrt{s_{\rm NN}} = 2.76$ TeV.

As shown in Fig. 2 the transverse momentum distribution of the $\psi(2S)$ is found to be as large as that of the J/ψ when they are initially produced from charm quarks by recombination. Accordingly, the transverse momentum distribution of the $\psi(2S)$ is still comparable to that of the J/ψ though major

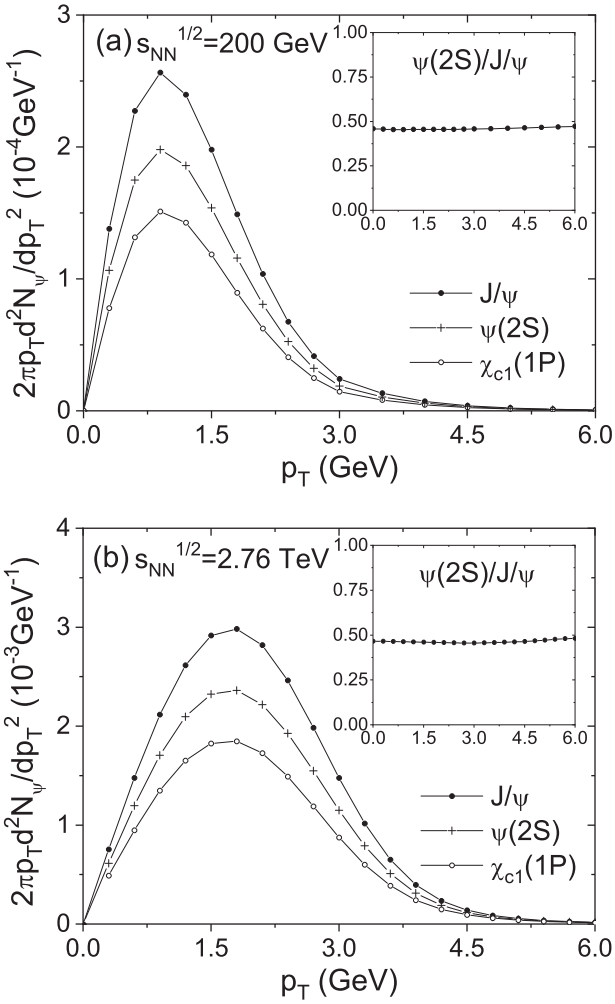

FIG. 2. Transverse momentum distributions multiplied by $2\pi\, p_T$, dN/dp_T of charmonium states J/ψ, $\chi_{c1}(1P)$, and $\psi(2S)$ mesons at midrapidity in 0–10 % centrality without feed-down contributions at (a) RHIC $\sqrt{s_{\rm NN}} = 200$ GeV and (b) LHC $\sqrt{s_{\rm NN}} = 2.76$ TeV. In the inset of each figure the transverse momentum distribution ratios between the $\psi(2S)$ and J/ψ obtained after including the feed-down contributions following Eq. (12) $d^2N_{\psi(2S)}/dp_T^2/d^2N^{\rm all}_{J/\psi}/dp_T^2$, are shown.

feed-down contributions to the J/ψ from heavier charmonium states, the $\chi_{c1}(1P)$ and $\psi(2S)$ are included, as shown in the inset of the Fig. 2. It is expected, however, that the actual transverse momentum distributions of the J/ψ measured at both RHIC and LHC would be slightly larger than those shown in Fig. 2 due to feed-down contributions from much heavier charmed and bottomed hadrons at higher transverse momentum regions.

It should be reminded that the yield, or the transverse momentum distribution of the $\psi(2S)$, is expected to be smaller than that of the J/ψ by about a factor of 10^2 in the statistical hadronization model where the heavier mass of the $\psi(2S)$ than that of the J/ψ by about 600 MeV makes the yield of the $\psi(2S)$ much smaller compared to that of the J/ψ. However, as seen in Fig. 2, the transverse momentum distribution of the $\psi(2S)$ based on the charm quark coalescence is not so small compared to that of the J/ψ meson, and therefore the transverse momentum distribution ratios between the $\psi(2S)$ and J/ψ meson becomes about 0.5 in the transverse momentum range between 0 and 6 GeV at both RHIC $\sqrt{s_{\rm NN}} = 200$ GeV and LHC $\sqrt{s_{\rm NN}} = 2.76$ TeV. This becomes more evident if the yield of the $\psi(2S)$ is directly compared to that of the J/ψ. Here I take the integration of the transverse momentum distribution of charmonium states shown in Fig. 1 over all transverse momenta, and evaluate yields of charmonium states. I take into account all the feed-down contribution as well for the yield based on Eq. (12), and summarize the result in Table II.

TABLE II. Total yields of the J/ψ, $\psi(2S)$, and $\chi_{c1}(1P)$ meson at a unit midrapidity interval $|y| < 0.5$ in 0–10 % centrality obtained by integrating the transverse momentum distributions shown in Fig. 1 over all transverse momenta at RHIC in $\sqrt{s_{\rm NN}} = 200$ GeV Au+Au collisions and at LHC in $\sqrt{s_{\rm NN}} = 2.76$ TeV Pb+Pb collisions.

	RHIC	LHC
J/ψ	7.6×10^{-4}	1.3×10^{-2}
$\psi(2S)$	3.5×10^{-4}	5.8×10^{-3}
$\chi_{c1}(1P)$	3.0×10^{-4}	5.1×10^{-3}

One can note in Table II that the yield of the $\psi(2S)$ is smaller than that of the J/ψ but is not so small as expected. It has been found that the reason for the enhanced production of the $\psi(2S)$ meson compared to the expectation in the statistical hadronization model is attributable to the large contribution at low transverse momenta from the wave function distribution of the $\psi(2S)$ in a momentum space [19]. I discuss in detail in Sec. IV what makes it possible for the yield and transverse momentum distribution of the $\psi(2S)$ to be half as large as those of the J/ψ meson.

III. ELLIPTIC AND TRIANGULAR FLOW OF CHARMONIUM STATES

I now discuss harmonic flows of charmonium states, i.e., the elliptic and triangular flow of the J/ψ, $\psi(2S)$, and $\chi_{c1}(1P)$ meson in heavy ion collisions. The flow harmonics are represented in general as v_n, the nth coefficient in the Fourier expansion of flows defined as [18,20]

$$v_n(p_T) = \langle \cos[n(\psi - \Psi_n)] \rangle = \frac{\int d\psi \cos[n(\psi - \Psi_n)] \frac{d^2N}{dp_T^2}}{\int d\psi \frac{d^2N}{dp_T^2}}, \tag{13}$$

where p_T and ψ are, respectively, the transverse momentum and azimuthal angle of the charmonium state in the transverse plane perpendicular to the collision axis. The Ψ_n in Eq. (13) is the event-plane angle, [25,26],

$$\Psi_n = \frac{1}{n} \tan^{-1} \left(\frac{\langle p_T \sin(n\psi) \rangle}{\langle p_T \cos(n\psi) \rangle} \right), \tag{14}$$

defined in the region, $-\pi/n < \Psi_n < \pi/n$. $\langle \cdots \rangle$ in Eq. (14) represents the average over particles.

In order to evaluate the elliptic and triangular flow of charmonium states, Eq. (13) I adopt the transverse momentum distributions of charmonium states, d^2N/dp_T^2, evaluated in Eq. (9). Then, the flow harmonics of charmonium states in Eq. (13) are dependent on flow harmonics of charm quarks via transverse momentum spectrum of charm quarks in Eq. (9),

$$\frac{d^2N_c}{dp_{cT}^2} = \frac{1}{2\pi p_{cT}} \frac{dN_c}{dp_{cT}} \left(1 + \sum_{n=1}^{\infty} 2v_{nc}(p_{cT}) \cos[n(\phi_c - \Psi_n)] \right), \tag{15}$$

where ϕ_c is an azimuthal angle of a charm quark in the transverse plane satisfying the momentum conservation condition in the process of charmonium production, $\vec{p}_{cT} + \vec{p}_{\bar{c}T} = \vec{p}_T$, in Eq. (9). $v_{nc}(p_{cT})$ in Eq. (15) is the nth flow harmonic of a charm quark.

Therefore, it is also necessary to know the information on the elliptic and triangular flow of a charm quark in order to evaluate the elliptic and triangular flow of charmonium states. I adopt here two kinds of flow harmonics of a charm quark obtained by the POWLANG transport analysis [43], which describes time evolutions of heavy quarks in heavy ion collisions through the relativistic Langevin equation.

It would be more consistent if the transverse momentum spectrum and flow harmonics of charm quarks have the same origin; I combine here the charm quark transverse momentum distribution, which were parametrized from the solution based on the relativistic Boltzmann equation [38], and the flow harmonics of a charm quark, which were obtained separately from the transport analysis [43]. I leave the study on this issue and the evaluation of more consistent elliptic and triangular flow of charmonium states for future research.

In the POWLANG transport study [43] the time evolution of charm-quark flow harmonics has been investigated, and transverse momentum distributions of charm-quark elliptic and triangular flow have been obtained for two occasions depending on the transport coefficient, κ, governing the momentum broadening during the propagation of heavy quarks in the medium; one is the weak coupling transport coefficient based on hard thermal loop (HTL) resummation analysis, and the other is the transport coefficient based on nonperturbative lattice quantum chromodynamics (QCD) calculation.

In this work I apply charm quark flow harmonics obtained by both transport coefficients in order to investigate flow harmonics of charmonium states. I show in Fig. 3 elliptic and triangular flow of charm quarks at RHIC $\sqrt{s_{\rm NN}} = 200$ GeV and LHC $\sqrt{s_{\rm NN}} = 5.02$ TeV from the POWLANG analysis based on HTL and lattice QCD (lQCD) transport coefficients [43] together with the fit for those flow harmonics in the Padé approximation,

$$v_{nc}(p_{cT}) = \frac{a_3 p_{cT}^3 + a_2 p_{cT}^2 + a_1 p_{cT}}{b_4 p_{cT}^4 + b_3 p_{cT}^3 + b_2 p_{cT}^2 + b_1 p_{cT} + 1}, \tag{16}$$

with $a_i (i = 1, 2, 3)$ and $b_j (j = 1, 2, 3, 4)$ being fit parameters. In Eq. (16), flow harmonics are parameterized to be zero at both $p_{cT} = 0$ and $p_{cT} \to \infty$ limits.

One can observe in Fig. 3 that flow harmonics based on the lattice QCD have peaks at low transverse momenta whereas those based on the HTL have peaks at higher transverse momenta. It has been found that the HTL transport coefficient gives rise to larger flow harmonics at high transverse

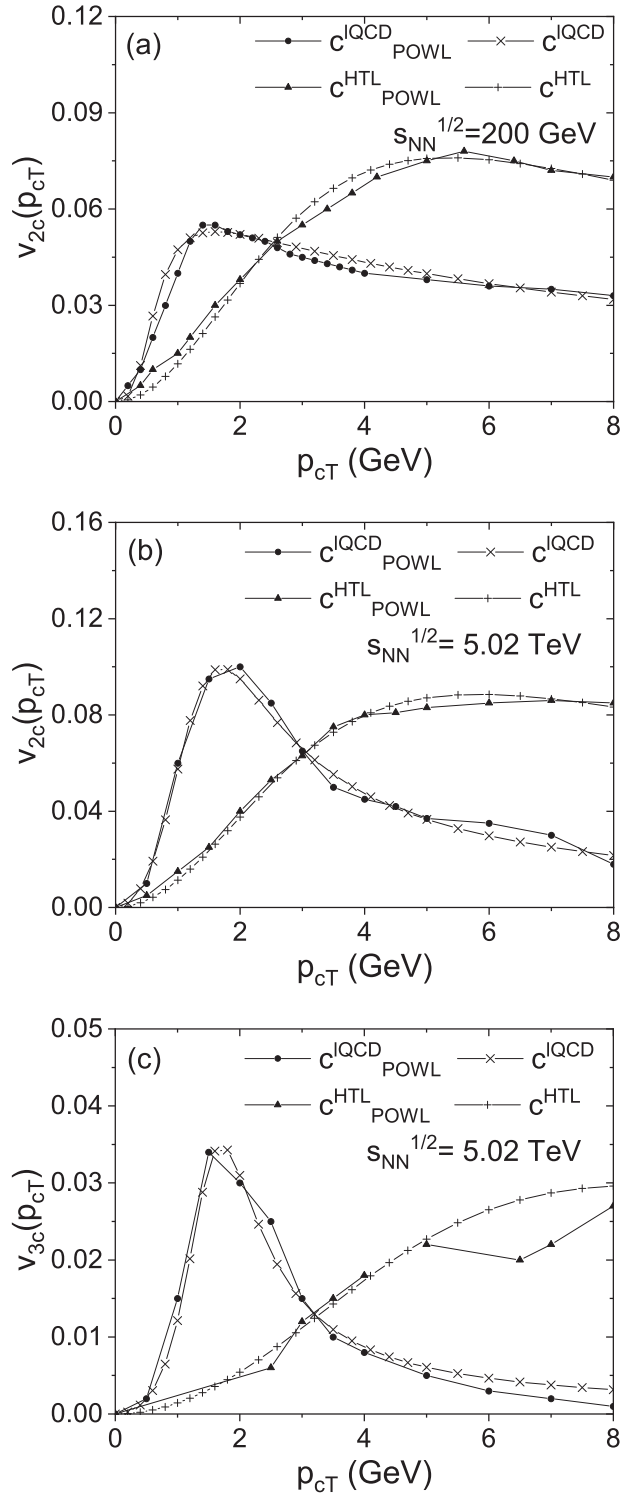

FIG. 3. (a) Elliptic flow of charm quarks at RHIC $\sqrt{s_{\rm NN}} =$ 200 GeV and (b) elliptic and (c) triangular flow of charm quarks at LHC $\sqrt{s_{\rm NN}} = 5.02$ TeV from the POWLANG transport setup based on HTL and lattice QCD (lQCD) transport coefficients [43], together with curve fits for those flow harmonics in the Padé approximation.

momentum region due to the parton energy loss, which is different in longitudinal and transverse directions, while the lattice QCD transport coefficient leads to the larger flow harmonics at low transverse momentum region due to the larger momentum diffusion constant [43]. Since the coalescence production of charmonium states are dominant at low and intermediate transverse momentum regions, it is expected that flow harmonics of charm quarks based on the lattice QCD play more important roles in understanding the flow harmonics of charmonium states.

It should be noted that the elliptic flow of charm quarks shown in Fig. 3(a) has been evaluated in centrality 0–80 % at RHIC $\sqrt{s_{\rm NN}} = 200$ GeV, and the elliptic and triangular flow of charm quarks displayed in Fig. 3(b) and 3(c) have been evaluated in 30–50 % centrality class at LHC, $\sqrt{s_{\rm NN}} =$ 5.02 TeV in the POWLANG analysis [43]. On the other hand, the transverse momentum distribution of charm quarks adopted here, $d^2N_c^L/dp_{cT}^2$ in Eq. (11) have been obtained at midrapidity in 0–10 % centrality at RHIC $\sqrt{s_{\rm NN}} = 200$ GeV, and also at midrapidity in 0–10 % centrality at LHC $\sqrt{s_{\rm NN}} =$ 2.76 TeV, desirable for the evaluation of both the transverse momentum distribution, Eq. (9) and flow harmonics of charmonium states, Eq. (13) at midrapidity in 0–10 % centrality.

Therefore, I adjust oscillator frequencies in order to make the transverse momentum distribution of charm quarks, Eq. (11) applicable for describing the transverse momentum distribution of charmonium states at both RHIC $\sqrt{s_{\rm NN}} =$ 200 GeV at midrapidity in 0–80 % centrality and LHC $\sqrt{s_{\rm NN}} = 5.02$ TeV also at midrapidity in 20–40 % centrality.

Comparing the transverse momentum distribution of the J/ψ evaluated with Eqs. (9)–(11) to the experimental measurement of the J/ψ transverse transverse momentum distribution at low transverse momentum region in Fig. 1 I obtain new oscillator frequencies, 0.024 GeV in centrality 0–80 % at RHIC and 0.020 GeV in 20–40 % centrality at LHC.

Shown in Fig. 4 are transverse momentum distributions, d^2N/dp_T^2 of charmonium states, the J/ψ, $\psi(2S)$, and $\chi_c(1P)$ meson at midrapidity in 0–80 % centrality at RHIC $\sqrt{s_{\rm NN}} =$ 200 GeV and those multiplied by $2\pi p_T$, dN/dp_T at midrapidity in 20–40 % centrality at LHC $\sqrt{s_{\rm NN}} = 5.02$ TeV evaluated with new oscillator frequencies, $\omega = 0.024$ and 0.020 GeV for RHIC and LHC, respectively. I have considered also the feed-down contribution from heavier charmonium states $\psi(2S)$ and $\chi_c(1P)$ mesons in adjusting oscillator frequencies for the transverse momentum distribution of the J/ψ. Also shown in Fig. 4 are experimental measurements of the J/ψ transverse momentum distribution at RHIC $\sqrt{s_{\rm NN}} = 200$ GeV at midrapidity in 0–80 % centrality [40] and the transverse momentum distribution of the J/ψ multiplied by $2\pi p_T$, dN/dp_T measured at LHC $\sqrt{s_{\rm NN}} = 5.02$ TeV, $|y| < 0.9$ in 20–40 % centrality [41].

As shown in Fig. 4 the reasonable agreement has been made between the experimental measurements and the evaluation of the J/ψ transverse momentum distribution up to about $p_T = 2$ GeV. One can note that at high transverse momentum region the transverse momentum distribution of the J/ψ does not agree well with the experimental measurements, owing to the non-negligible contributions to the J/ψ production at higher transverse momenta from the decay of heavier bottomed hadrons, which are not taken into account in the present analysis.

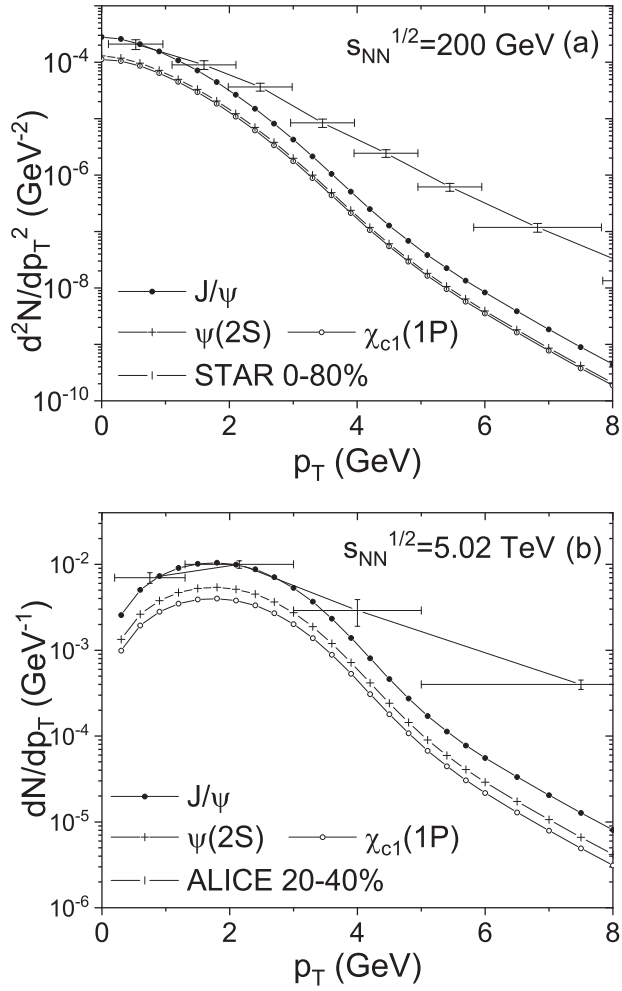

FIG. 4. (a) Transverse momentum distributions, d^2N/dp_T^2 of charmonium states at midrapidity in 0–80 % centrality at RHIC $\sqrt{s_{\rm NN}} = 200$ GeV and (b) those multiplied by $2\pi p_T$, dN/dp_T at midrapidity in 20–40 % centrality at LHC $\sqrt{s_{\rm NN}} = 5.02$ TeV evaluated with new oscillator frequencies, $\omega = 0.024$ and 0.020 for RHIC and LHC, respectively. I also show experimental measurements of the J/ψ transverse momentum distribution at RHIC $\sqrt{s_{\rm NN}} =$ 200 GeV [40] at midrapidity in 0–80 % centrality (a) and the transverse momentum distribution of the J/ψ multiplied by $2\pi p_T$, dN/dp_T measured at LHC $\sqrt{s_{\rm NN}} = 5.02$ TeV, $|y| < 0.9$ in centrality 20–40 % [41] (b).

The new oscillator frequencies, $\omega = 0.024$ and 0.020 GeV are smaller than those obtained previously, $\omega = 0.078$ and 0.076 GeV at RHIC and LHC, respectively, thereby giving rise to more production of charmonium states; charmonium states are expected to be more abundant as the centrality range is increased from 0–10 to 0–80 % at RHIC, and also as the collision energy is increased from $\sqrt{s_{\rm NN}} = 2.76$–5.02 TeV at LHC.

In addition to flow harmonics of charm quarks, it is also necessary to know the information on the event plane, Eq. (14), in order to evaluate the flow harmonics of charmonium states. One can clearly see that flow harmonics of

charmonium states, Eq. (13), are actually sensitive to the change of the event plane, Eq. (14). Experimentally, the event plane is determined from all hadrons observed in the same event based on the relation between the impact parameter and transverse plane. On the other hand, it has been argued that the event plane method may give rise to discrepancies from the true values, and thus the way of using the flow vector $\vec{Q}$ instead of evaluating the event plane has been suggested [44].

Therefore, I consider here event plane blind flow harmonics, or event-averaged flow harmonics of charmonium states; since the flow harmonics of charm quarks shown in Fig. 3 evaluated in the POWLANG transport study have also been averaged over events [43], it is also natural to consider here elliptic and triangular flow of charmonium states formed from those of charm quarks on the same condition that events are averaged,

$$v_n(p_T) = \frac{\frac{n}{2\pi}\int_{-\frac{\pi}{n}}^{\frac{\pi}{n}}\int d\psi \cos[n(\psi-\Psi_n)]\frac{d^2N}{dp_T^2}d\Psi_n}{\frac{n}{2\pi}\int_{-\frac{\pi}{n}}^{\frac{\pi}{n}}\int d\psi \frac{d^2N}{dp_T^2}d\Psi_n}. \quad (17)$$

Though the event-averaged triangular flow of charm quarks is adopted in evaluating that of charmonium states, the effects of event-by-event fluctuation on the triangular flow of charmonium states are taken into account here; triangular flow of charm quarks was obtained from collisions between nucleons in numerous different initial positions reflecting event-by-event fluctuation in the POWLANG transport study [43]. In that sense I adopt the event-by-event fluctuation effects on the triangular flow of charmonium states entirely from the charm quark triangular flow bearing the effects caused by different initial configurations of colliding nucleons.

With these in mind I calculate the elliptic and triangular flow of charmonium states at RHIC and LHC using both the transverse momentum distribution of charm quarks shown in Fig. 4 and flow harmonics of charm quarks shown in Fig. 3. As the transverse momentum distribution and flow harmonics of charm quarks at RHIC $\sqrt{s_{\rm NN}} = 200$ GeV are all prepared in the same centrality 0–80 %, I calculate consistently the elliptic flow of charmonium states in centrality 0–80 %. However, for the flow harmonics of charmonium states at LHC $\sqrt{s_{\rm NN}} =$ 5.02 TeV, I assume that flow harmonics of charm quarks in centrality 30–50 % are similar to those in centrality 20–40 % at LHC $\sqrt{s_{\rm NN}} = 5.02$ TeV, and calculate the elliptic and triangular flow of charmonium states in 20–40 % centrality at LHC $\sqrt{s_{\rm NN}} = 5.02$ TeV by combining the transverse momentum distribution of charm quarks in 20–40 % centrality shown in Fig. 4 with flow harmonics of charm quarks in centrality 30–50 % shown in Fig. 3.

Shown in Fig. 5(a) and 5(b) are the elliptic flows of charmonium states calculated from those of charm quarks based on, respectively, the lQCD and HTL transport coefficients in the POWLANG transport setup [43] at RHIC $\sqrt{s_{\rm NN}} =$ 200 GeV, together with the measurement of the J/ψ elliptic flow at the same RHIC top energy in rapidity $|y| < 1$ in 0–80 % centrality [45]. Also the elliptic flows of charmonium states calculated from those of charm quarks based on, respectively, the lQCD and HTL transport coefficients in the POWLANG transport at LHC $\sqrt{s_{\rm NN}} = 5.02$ TeV, are shown in Fig. 5(c) and 5(d), together with the measurement of the J/ψ elliptic flow at the same LHC energy in rapidity $|y| < 0.9$ in 20–40 % centrality [46]. Finally, shown in Fig. 5(e) and 5(f) are the triangular flows of charmonium states calculated from those of charm quarks based on, respectively, the lQCD and HTL transport coefficients in the POWLANG transport at LHC $\sqrt{s_{\rm NN}} = 5.02$ TeV, together with the measurement of the J/ψ triangular flow in the rapidity range of $2.5 < y < 4.0$ in 30–50 % centrality at the same LHC energy [47]. Also shown are corresponding flow harmonics of bare charm quarks in each figure for comparison.

As shown in Fig. 5, the elliptic flow at RHIC is smaller than that at LHC for the POWLANG analysis with the lQCD transport coefficients, while the elliptic flow at RHIC is similar to that at LHC for the POWLANG analysis with the HTL transport coefficients. When the medium is strongly coupled, the larger collision energy at LHC than at RHIC seems more effective in inducing charmonium states to flow within the medium. On the other hand, the collision energy does not matter too much for the flow of charmonium states in a weakly coupled medium.

One can see in Fig. 5 that the flow harmonics of charmonium states are dominant at low and intermediate transverse momentum regions when charm quarks interacts strongly with the medium at low transverse momenta or when the flow harmonics of charm quarks are adopted from the POWLANG transport analysis with the nonperturbative lQCD transport coefficient, Figs. 5(a), 5(c) and 5(e). On the other hand, the flow harmonics of charmonium states obtained with those of charm quarks prevalent at higher transverse momentum region due to the weak coupling transport coefficient based on HTL, continue to be generated at low and intermediate transverse momentum regions, as seen in Figs. 5(b), 5(d) and 5(f).

One can also notice in Fig. 5 that flow harmonics of charmonium states, the J/ψ, $\psi(2S)$, and $\chi_c(1P)$ meson are almost the same at both RHIC and LHC, irrespective of the two occasions, i.e., flow harmonics of constituent charm quarks situated in two different interactions with the medium, governed by the lQCD and HTL transport coefficients in the POWLANG transport analysis.

It is reasonable to expect that the elliptic and triangular flow of different charmonium states are different owing to the different transverse momentum distribution, Eq. (13) originated from the different internal structures of charmonium states, or the different wave function distribution in momentum space, Eq. (10). However, even though the transverse momentum distributions are different for each charmonium state as shown in Fig. 2, the elliptic and triangular flow of different charmonium states are found to be almost the same in the entire transverse momentum range.

I find that the reason why I obtain almost the same flow harmonics for charmonium states, the J/ψ, $\psi(2S)$, and $\chi_c(1P)$ meson, is due to the characteristics of the v_n itself. Since the v_n in Eq. (13) is the average of cosine functions in different orders n over transverse momentum with the weight of the transverse momentum distribution of charmonium states, the contribution of transverse momentum distributions originated from the different internal structures of charmonium states are averaged out for all charmonium states.

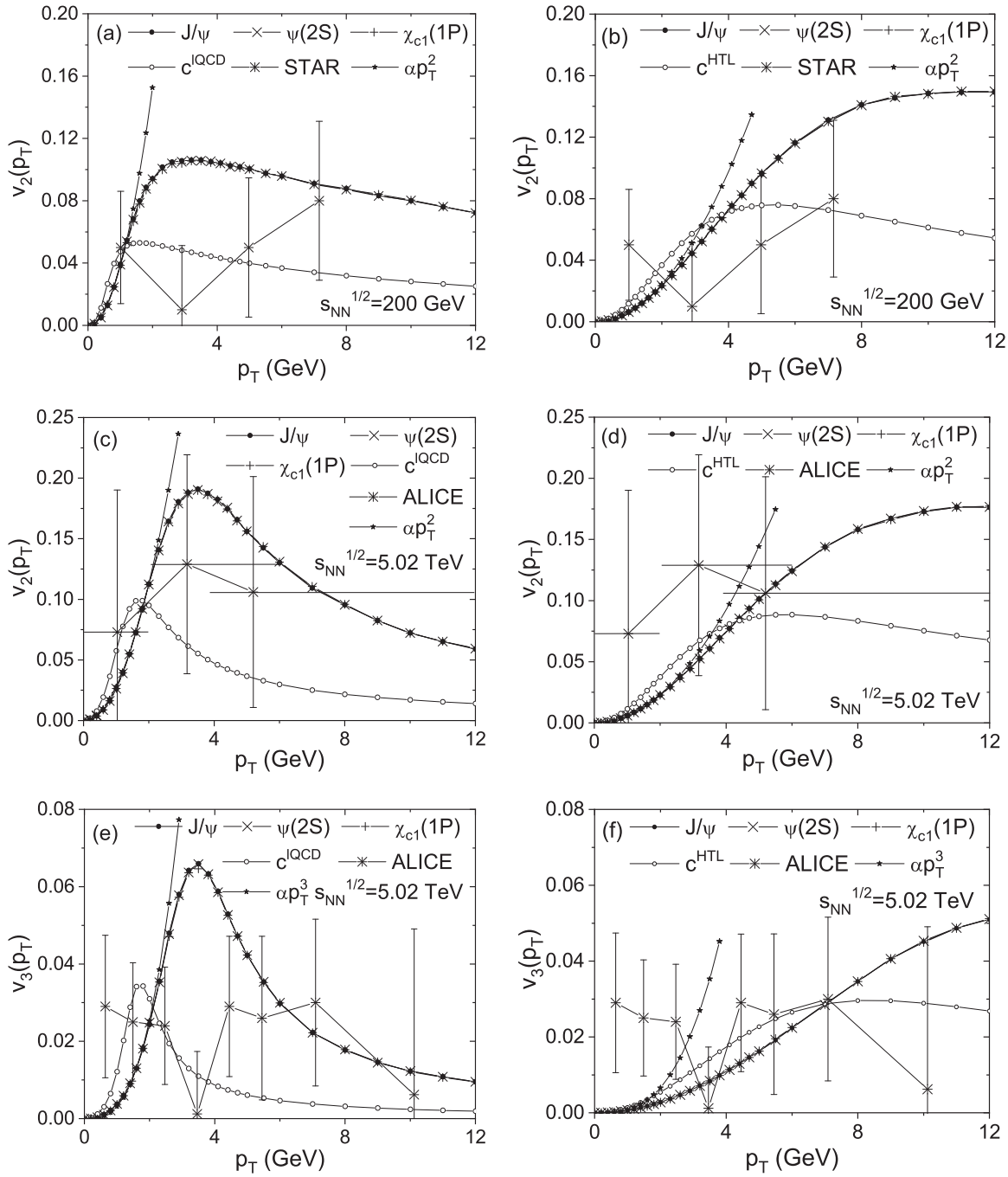

FIG. 5. Elliptic flows of charmonium states calculated from those of charm quarks based on the (a) lQCD and (b) HTL transport coefficients in the POWLANG transport setup [43] at RHIC $\sqrt{s_{\rm NN}} = 200$ GeV, together with the measurement of the J/ψ elliptic flow at the same RHIC top energy in rapidity $|y| < 1$ in 0–80 % centrality [45]. Also, elliptic flows of charmonium states calculated from those of charm quarks based on the (c) lQCD and (d) HTL transport coefficients in the POWLANG transport at LHC $\sqrt{s_{\rm NN}} = 5.02$ TeV, together with the measurement of the J/ψ elliptic flow at the same LHC energy in rapidity $|y| < 0.9$ in 20–40 % centrality [46]. Finally, triangular flows of charmonium states calculated from those of charm quarks based on the (e) lQCD and (f) HTL transport coefficients in the POWLANG transport at LHC $\sqrt{s_{\rm NN}} = 5.02$ TeV, together with the measurement of the J/ψ triangular flow in rapidity range of $2.5 < y < 4.0$ in 30–50 % centrality at the same LHC energy [47]. I also show the corresponding flow harmonics of bare charm quarks in each figure for comparison.

One can see the explicit dependence of both the numerator and denominator part of v_n in Eq. (13) on the internal structure or the wave function distribution in the momentum space of each charmonium state. Nevertheless, the flow harmonics of all charmonium states become almost identical when those are evaluated by the definition of v_n in Eq. (13). The similar amounts of contribution to both the numerator and denominator of the v_n from different transverse momentum distributions

TABLE III. Fitting functions of the J/ψ meson v_n at low transverse momentum region, αp_T^n shown in Fig. 5 at RHIC $\sqrt{s_{\rm NN}} = 200$ GeV and LHC $\sqrt{s_{\rm NN}} = 5.02$ TeV.

	RHIC		LHC			
	n=2		n=2		n=3	
αp_T^n	lQCD	HTL	lQCD	HTL	lQCD	HTL
α	0.038	0.0061	0.028	0.0058	0.0032	0.00082

of charmonium states are canceled out of each other, resulting in almost the same flow harmonics for all charmonium states. I discuss this issue in detail in Sec. IV.

Since it has been found that the elliptic flow at low transverse momentum region is close to the square function of the transverse momentum, p_T^2, and similarly, the triangular flow also at low transverse momentum region is close to the cube function of p_T, p_T^3 [48] I also show in Fig. 5 the square and cube function fits as functions of the p_T, αp_T^2, and αp_T^3 with parameters α summarized in Table III, in order to investigate the behavior of the elliptic and triangular flow at low transverse momentum region.

As shown in Fig. 5 the elliptic (triangular) flow obtained from that of charm quarks in the strongly coupled medium, or in the lQCD transport coefficients from the POWLANG analysis behaves like the p_T^2 (p_T^3) up to about $p_T = 2$ GeV, while the elliptic (triangular) flow obtained from that of charm quarks in the weakly coupled medium, or in the HTL transport coefficients from the POWLANG shows the similar behavior of the p_T^2 (p_T^3) up to about $p_T = 3$ ($p_T = 1$) GeV at low transverse momentum region. Considering that the v_n usually increases with p_T^n up to about $p_T = M$ for a hadron with its mass M [48], one finds that this tendency applies more suitably to charmonium states in a weakly coupled medium with the HTL transport coefficients from the POWLANG.

When recalling the relation between the flow coefficients and the interaction of constituent quarks with other quarks in QGP, one can expect that the elliptic flow of charmonium states increases steeply at p_T smaller than their corresponding masses M when charm quarks are in the medium with the nonperturbative lQCD transport coefficient in the POWLANG transport analysis. For the same reason, one can observe that the elliptic flow of charmonium states based on those of charm quarks prevailing at higher transverse momentum regions due to the weak coupling transport coefficients increases gradually with p_T^2 up to about their corresponding masses M. This tendency still holds for the triangular flow as shown in Fig. 5(e) and 5(f). I discuss further on this issue in Sec. IV.

Also presented in Fig. 6 are rescaled elliptic flows of charmonium states $v_2(p_T/NQ)/NQ = v_{2,c\bar{c}}(p_T/2)/2$ with the number of constituent quarks $NQ = 2$ calculated from those of charm quarks based on the lQCD [Fig. 6(a)] and HTL [Fig. 6(b)] transport coefficients in POWLANG transport setup [43] at RHIC $\sqrt{s_{\rm NN}} = 200$ GeV. Also, rescaled elliptic flows of charmonium states $v_2(p_T/2)/2$ calculated from those of charm quarks based on the lQCD [Fig. 6(c)] and HTL [Fig. 6(d)] transport coefficients in POWLANG transport setup [43] at LHC $\sqrt{s_{\rm NN}} = 5.02$ TeV are shown. Finally, rescaled triangular flows of charmonium states $v_3(p_T/2)/2$ calculated from those of charm quarks based on the lQCD [Fig. 6(e)] and HTL [Fig. 6(f)] transport coefficients in POWLANG transport setup [43] at LHC $\sqrt{s_{\rm NN}} = 5.02$ TeV are presented. Also shown are the corresponding flow harmonics of bare charm quarks $v_{2,c}(p_T)$ or $v_{3,c}(p_T)$ in each figure for comparison.

Reminding the well-known relation between the elliptic flow of mesons and that of constituent quarks $v_{2,M}(p_T) \approx 2v_{2,q}(p_T/2)$ [18,20], I notice that the elliptic flow of charmonium states satisfy the similar relation to that of charm quarks $v_{2,c\bar{c}}(p_T) \approx 2v_{2,c}(p_T/2)$; the transverse momentum at the peak in the elliptic flow of charmonium states is almost twice that at the peak position of the elliptic flow of charm quarks as shown in Figs. 5(a)–5(d). Similarly, I find that the above relation also holds for the triangular flow of charmonium states, $v_{3,c\bar{c}}(p_T) \approx 2v_{3,c}(p_T/2)$, as shown in Fig. 5(e) and 5(f).

IV. DISCUSSION

A. Dependence of charmonia production on their structures; J/ψ vs. $\psi(2S)$

Here, I discuss in more detail the cause of the larger production of the $\psi(2S)$, contrary to the statistical hadronization model expectation, and confirm that the yield of the $\psi(2S)$ must be large, as comparable as that of the J/ψ when charmonium states are produced from charm quarks by recombination at the quark-hadron phase transition.

Reminding that the hadron production by recombination is dominant at low transverse momentum region, one can expect that the larger contributions at lower transverse momentum from the squared wave function in momentum space $|\tilde{\psi}(p)|^2$ in Eq. (9) leads to a larger yield or a larger transverse momentum distribution. Therefore, the bigger peak, or the larger contribution in the charmonia wave function square in a momentum space, especially in the low transverse momentum region, is very crucial to the yield or transverse momentum distribution of charmonium states when they are produced from charm quarks by recombination.

Figure 7 displays the wave function distribution of J/ψ and $\psi(2S)$ mesons in both coordinate and momentum spaces. The squared wave functions in a coordinate space $|\psi(r)|^2$ for the J/ψ and $\psi(2S)$, and those in a momentum space $|\tilde{\psi}(p)|^2/(2\pi)^3$ for the J/ψ and $\psi(2S)$ are also shown in the inset of Fig. 7(a), and in the inset of Fig. 7(b), respectively. The superscript G implies a Gaussian or a harmonic oscillator wave function adopted in constructing the Wigner function, Eq. (10).

Since the $\psi(2S)$ is a radially excited state of the J/ψ, the wave function of the $\psi(2S)$ has one node as shown in Fig. 7(a). Therefore, the squared wave function in a coordinate space $|\psi(r)|^2$ of the $\psi(2S)$ has two peaks; the bigger one is located near the center, and the smaller one is on the right-hand side of the node, as shown in the inset of Fig. 7(a). On the other hand, the wave function of the J/ψ is localized near the center without a node in a coordinate space, resulting in

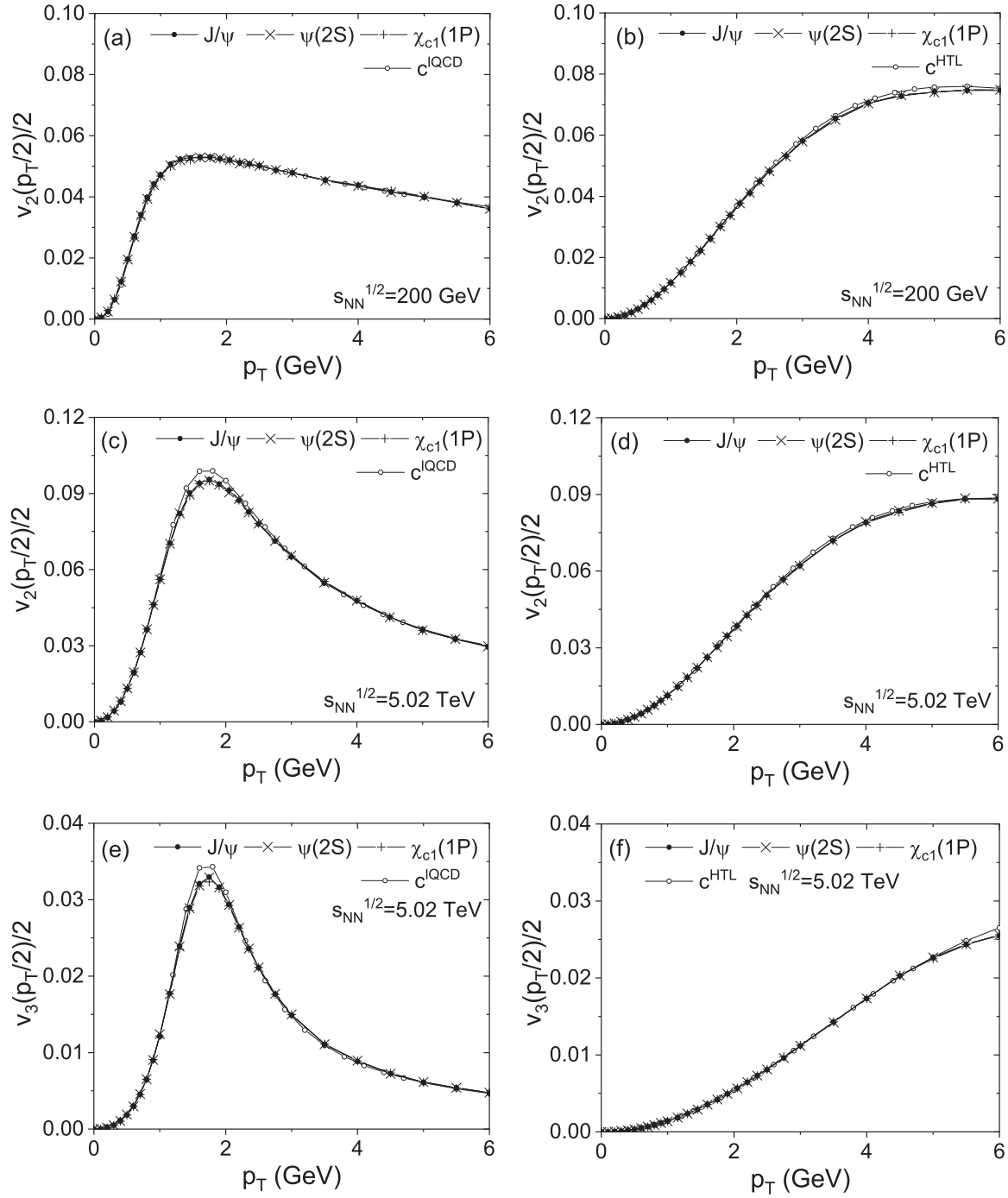

FIG. 6. I present rescaled elliptic flows of charmonium states, $v_2(p_T/2)/2 = v_{2,c\bar{c}}(p_T/NQ)/NQ$ with the number of constituent quarks, $NQ = 2$ calculated from those of charm quarks based on the (a) lQCD and (b) HTL transport coefficients in POWLANG transport setup [43] at RHIC $\sqrt{s_{\rm NN}} = 200$ GeV. Also, rescaled elliptic flows of charmonium states, $v_2(p_T/2)/2$ calculated from those of charm quarks based on the (c) lQCD and (d) HTL transport coefficients in POWLANG transport setup [43] at LHC $\sqrt{s_{\rm NN}} = 5.02$ TeV are shown. Finally, rescaled triangular flows of charmonium states, $v_3(p_T/2)/2$ calculated from those of charm quarks based on the (e) lQCD and (f) HTL transport coefficients in POWLANG transport setup [43] at LHC $\sqrt{s_{\rm NN}} = 5.02$ TeV are presented. I also show the corresponding flow harmonics of bare charm quarks $v_{2,c}(p_T)$ or $v_{3,c}(p_T)$ in each figure for comparison.

one peak in the $|\psi(r)|^2$ for the J/ψ in a coordinate space, as also shown in the inset of Fig. 7(a).

These differences in the wave function of the J/ψ and $\psi(2S)$ in a coordinate space play significant roles in making their production different through the wave function distribution in a momentum space; the wave function distributions in a coordinate space can be Fourier transformed into those in a momentum space as shown in Fig. 7(b), and it is the squared

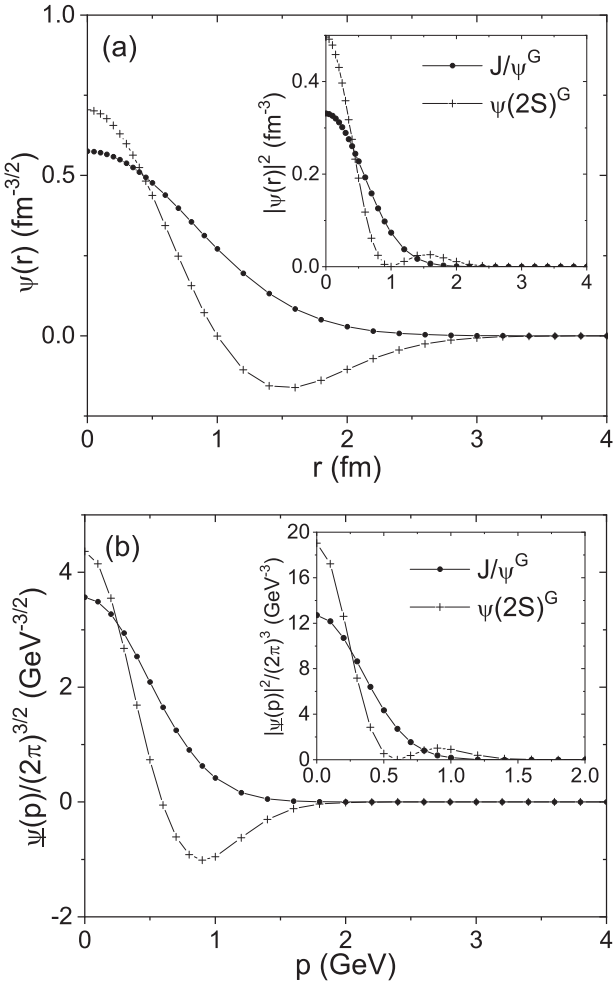

FIG. 7. (a) Gaussian wave function distributions of the J/ψ and $\psi(2S)$ in a coordinate space, and (b) those of the J/ψ and $\psi(2S)$ divided by $(2\pi)^{3/2}$ in a momentum space. In the inset of the figure (a) the wave function squares in a coordinate space, $|\psi(r)|^2$ for the J/ψ and $\psi(2S)$ are shown. Also in the inset of figure (b) the wave function squares in a momentum space $|\tilde{\psi}(p)|^2/(2\pi)^3$ for the J/ψ and $\psi(2S)$ are shown.

wave function in a momentum space, $|\tilde{\psi}(k)|^2$ that contributes differently to the production yield, or the transverse momentum distribution for the J/ψ and $\psi(2S)$ as shown in Eq. (9).

Looking into the wave function of the $\psi(2S)$ in a momentum space in more detail, one still finds in Fig. 7(b) one node as in that of the $\psi(2S)$ in a coordinate space. One can also notice that the squared wave function of the $\psi(2S)$ is even bigger than that of the J/ψ near the zero transverse momentum, causing a bigger peak in the squared wave function of the $\psi(2S)$ compared to the peak in the J/ψ squared wave function in the lower transverse momentum region as shown in the inset of Fig. 7(b).

The transverse momentum of charm quarks in a fireball frame, hidden in the squared wave function $|\tilde{\psi}(k)|^2$, Eq. (9), via the relative momentum between charm quarks $\vec{k} = (\vec{p}^{\,'}_{cT} - \vec{p}^{\,'}_{\bar{c}T})/2$ in the charmonium frame, is integrated out together with the transverse momentum distribution of charm and anticharm quarks, resulting in the transverse momentum distribution of charmonium states. In this respect, the larger peak in the squared wave function of the $\psi(2S)$ in a momentum space at low transverse momentum region is attributable to the larger production of the $\psi(2S)$, thereby the yield or transverse momentum distribution of the $\psi(2S)$ are half as large as those of the J/ψ.

B. Dependence of elliptic and triangular flows of charmonium states on their structures

I discuss in this section the dependence of elliptic and triangular flows of charmonium states on their internal structures. Since the flow harmonics of charmonium states are dependent on their internal structures via their transverse momentum distributions, it seems natural to observe different elliptic and triangular flows originated from different transverse momentum distributions for different charmonium states. However, as shown in Fig. 5 almost same flow harmonics for all charmonium states, the J/ψ, $\psi(2S)$, and $\chi_c(1P)$ have been obtained at both RHIC and LHC, regardless of two different charm quark interactions with the medium, the lQCD and HTL transport coefficients in the POWLANG transport analysis.

Noting that the v_n in Eq. (17) is the average of cosine functions in different orders n over the transverse momentum with the weight of the transverse momentum distribution of charmonium states, I investigate separately the dependence of numerator and denominator parts of the elliptic flow v_2 on their internal structures or their wave function distributions. I denote the numerator and denominator part of v_2 as v_{2N} and v_{2D}, respectively, from Eq. (17),

$$v_{2N}(p_T) = \frac{2}{2\pi}\int_{-\frac{\pi}{2}}^{\frac{\pi}{2}}\int d\psi\,\cos[2(\psi-\Psi_2)]\frac{d^2N}{dp_T^2}d\Psi_2$$
$$v_{2D}(p_T) = \frac{2}{2\pi}\int_{-\frac{\pi}{2}}^{\frac{\pi}{2}}\int d\psi\frac{d^2N}{dp_T^2}d\Psi_2. \quad (18)$$

Shown in Fig. 8 are numerator parts of the elliptic flow $v_{2N}(p_T)$, Eq. (18), for charmonium states, i.e., the J/ψ, $\psi(2S)$, and $\chi_{c1}(1P)$ at LHC $\sqrt{s_{\rm NN}} = 5.02$ TeV in the lQCD [Fig. 8(a)] and HTL [Fig. 8(c)] transport coefficients in POWLANG transport setup [43]. Also shown in Fig. 8 are denominator parts of the elliptic flow $v_{2D}(p_T)$, Eq. (18) of the J/ψ, $\psi(2S)$, and $\chi_{c1}(1P)$ meson at LHC $\sqrt{s_{\rm NN}} = 5.02$ TeV in the lQCD [Fig. 8(b)] and HTL [Fig. 8(d)] transport coefficients in POWLANG transport setup. Here, the feed-down contributions, Eq. (12) from heavier charmonium states are not taken into account in both $v_{2N}(p_T)$ and $v_{2D}(p_T)$ of the J/ψ, $\psi(2S)$, and $\chi_{c1}(1P)$. One can clearly see different v_{2D} as well as v_{2N} for different charmonium states, showing the explicit dependence of both v_{2N} and v_{2D} of the J/ψ, $\psi(2S)$, and $\chi_c(1P)$ meson on their transverse momentum distributions.

The numerator part of v_2 is similar to the transverse momentum distribution multiplied by $2\pi p_T$ as shown in Fig. 2; the v_{2N} is larger in the order of the J/ψ, $\psi(2S)$, and $\chi_c(1P)$ due to their transverse momentum distributions as expected.

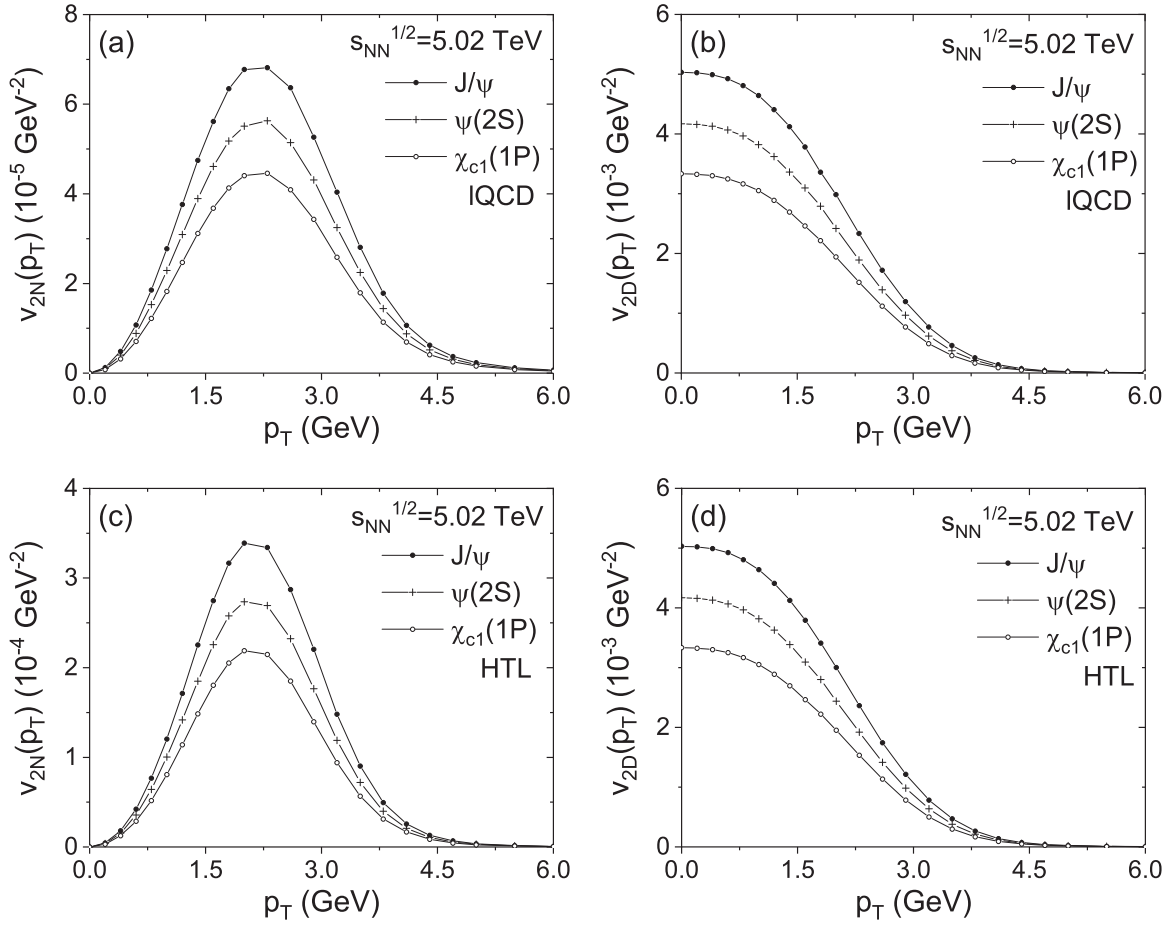

FIG. 8. Numerator parts of the elliptic flow in Eq. (17) denoted by $v_{2N}(p_T)$ for charmonium states, i.e., the J/ψ, $\psi(2S)$, and $\chi_{c1}(1P)$ at LHC $\sqrt{s_{\rm NN}} = 5.02$ TeV in the (a) lQCD and (c) HTL transport coefficients in POWLANG transport setup [43] are shown. Also shown are denominator parts of the elliptic flow in Eq. (17) denoted by $v_{2D}(p_T)$ of the J/ψ, $\psi(2S)$, and $\chi_{c1}(1P)$ meson at LHC $\sqrt{s_{\rm NN}} = 5.02$ TeV in the (b) lQCD and (d) HTL transport coefficients in POWLANG transport setup.

The shape of both figures is also similar, though the unit in each figure is different. The behavior of v_{2N} as a function of p_T is entirely affected by the sum of a charm and an anticharm quark v_{2c} in the coalescence, $\sim(v_{2c} + v_{2\bar{c}})$, Eq. (15).

The same characteristics observed in the numerator part of v_2 are also found in the denominator part of v_2; the v_{2D} is larger in the order of the J/ψ, $\psi(2S)$, and $\chi_c(1P)$ originated from their transverse momentum distributions. In addition, one can note that the v_{2D} of charmonium states is almost similar to the transverse momentum distribution itself as shown in Fig. 1. One can understand this as the v_{2D} is reflected by the factor $\sim(1 + 2v_{2c}v_{2\bar{c}})$ in the coalescence of a charm and an anticharm quarks, Eq. (15), and both the v_{2c} and $v_{2\bar{c}}$ are as small as a few percent, as shown in Fig. 3.

As discussed so far, the denominator as well as numerator parts of v_2 is explicitly dependent on the transverse momentum distribution. However, each dependence of both the numerator and denominator on the transverse momentum distribution is canceled out when v_2 is obtained. For this reason, one finds no differences in the v_n of the J/ψ, $\psi(2S)$, and $\chi_c(1P)$ meson in spite of their different wave function distributions, as shown in Fig. 5.

C. Elliptic and triangular flows of charmonium states at low transverse momentum regions

I discuss here the elliptic and triangular flows of charmonium states at low transverse momentum region. It has been found that the elliptic flow at low transverse momentum regions behaves like the square function of transverse momentum, p_T^2, and similarly the triangular flow at low transverse momentum regions behaves as the cube function of p_T, p_T^3 [48].

If the elliptic flow behaves as p_T^2 at low transverse momentum region $v_2^{1/2}/p_T$ is expected to be a constant as a function of transverse momentum at low p_T. Therefore, in order to investigate the elliptic and triangular flows at low transverse momentum regions $v_n^{1/n}/p_T$ have been measured for the J/ψ [47] as well as light particles [49] as functions of p_T.

Shown in Fig. 9 are plots of $v_n^{1/n}/p_T$ together with $v_n^{1/n}$ for the J/ψ meson at LHC $\sqrt{s_{\rm NN}} = 5.02$ TeV evaluated with the charm quark elliptic and triangular flow from the POWLANG transport setup in the lQCD [Figs. 9(a), 9(c)] and HTL [Figs. 9(b), 9(d)] transport coefficients. Also shown are plot $v_n^{1/n}$ as well as $v_n^{1/n}/p_T$ of bare charm quark elliptic and

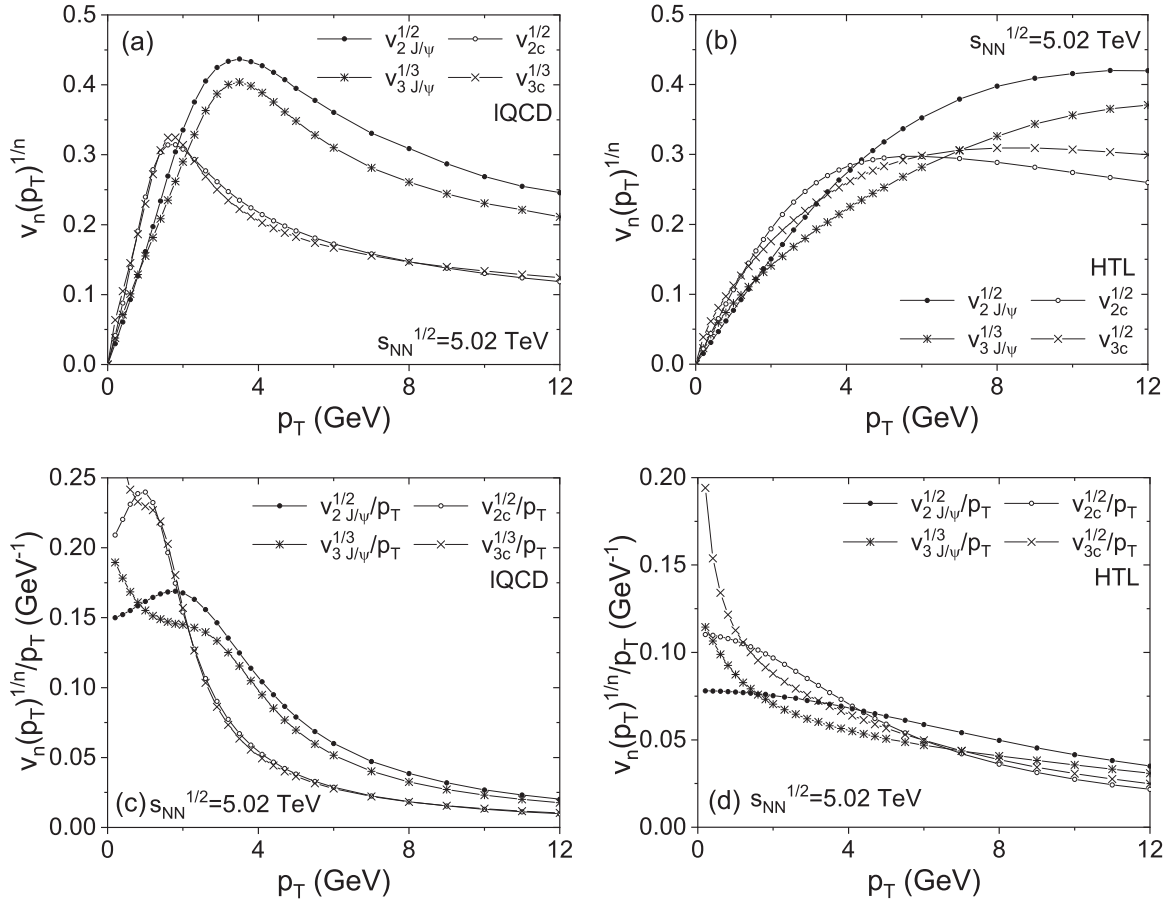

FIG. 9. Plots of $v_n^{1/n}/p_T$ together with $v_n^{1/n}$ for the J/ψ meson at LHC, $\sqrt{s_{\rm NN}} = 5.02$ TeV evaluated with the charm quark elliptic and triangular flow from the POWLANG transport setup in the (a), (c) lQCD and (b), (d) HTL transport coefficients. Plots of $v_n^{1/n}$ as well as $v_n^{1/n}/p_T$ of bare charm quark elliptic and triangular flow obtained from two cases in the POWLANG transport setup as a function of transverse momenta are also shown in each figure for comparison.

triangular flow obtained from two cases in the POWLANG transport setup shown in Fig. 3 as functions of transverse momenta for comparison.

As shown in the previous section, the relation between the flow harmonics of mesons and that of constituent quarks, i.e., $v_{n,J/\psi}(p_T) \approx 2v_{n,c}(p_T/2)$, holds for charmonium states. One can see in Fig. 9 that the $v_n^{1/n}/p_T$ and $v_n^{1/n}$ of the J/ψ also reflects that of bare charm quarks via the above relation $v_{n,J/\psi}(p_T) \approx 2v_{n,c}(p_T/2)$. Nevertheless, one can observe that the above relation holds differently at low and intermediate transverse momentum regions for the elliptic and triangular flow depending on interaction strength between charm quarks and the medium.

Focusing on the $v_n^{1/n}/p_T$, one finds that it is not a constant at low transverse momentum region in a strongly coupled medium with the lQCD transport coefficient in POWLANG, as shown in Fig. 9(c). The triangular flow of the J/ψ, $v_3^{1/3}/p_T$ in a weakly coupled medium with the HTL transport coefficient is not also a constant, whereas the elliptic flow of the J/ψ, $v_2^{1/2}/p_T$ is found to be a constant up to about 3 GeV as shown in Fig. 9(d).

Even though I obtain at low transverse momentum region the best fit functions of p_T^2 or p_T^3 for the elliptic and triangular flow, Fig. 5 and Table III, I find that the $v_n^{1/n}/p_T$ might not be a constant, which is possible as the fit function usually passes through between the data points. For example, the elliptic flow lies below the αp_T^2 fit function $\alpha^{1/2} = 0.028^{1/2} \approx 0.167$ up to about 1 GeV with the α from Table III, while that lies above the fit function between about 1 and 2 GeV, resulting in the increasing $v_2^{1/2}/p_T$ up to about 2 GeV as shown in Fig. 9(c). In the case of $v_2^{1/2}/p_T$ in the HTL transport coefficient shown in Fig. 9(d) the p_T^2 fit function describes almost exactly the elliptic flow of the J/ψ, leading to the constant $\alpha^{1/2} = 0.0058^{1/2} \approx 0.076$ up to about 3 GeV. It should be noted that the relation between the flow harmonics of the J/ψ and those of charm quarks, i.e., $v_{n,J/\psi}(p_T) \approx 2v_{n,c}(p_T/2)$, holds here; when the $v_n^{1/n}/p_T$ of charm quarks is not a constant at low transverse momenta, that of the J/ψ cannot be a constant at two times the low transverse momenta, as shown in Fig. 9.

When the above relation holds for the elliptic and triangular flow $v_{2,J/\psi}(p_T) \approx 2v_{2,c}(p_T/2)$ and $v_{3,J/\psi}(p_T) \approx 2v_{3,c}(p_T/2)$, the ratio $v_{2,J/\psi}^{1/2}(p_T)/v_{3,J/\psi}^{1/3}(p_T)$ is estimated to be about $2^{1/2}/2^{1/3}v_{2,c}^{1/2}(p_T/2)/v_{3,c}^{1/3}(p_T/2)$. As one sees in Fig. 9(a) that $v_{2,c}^{1/2}(p_T/2)$ is very similar to $v_{3,c}^{1/3}(p_T/2)$, one can

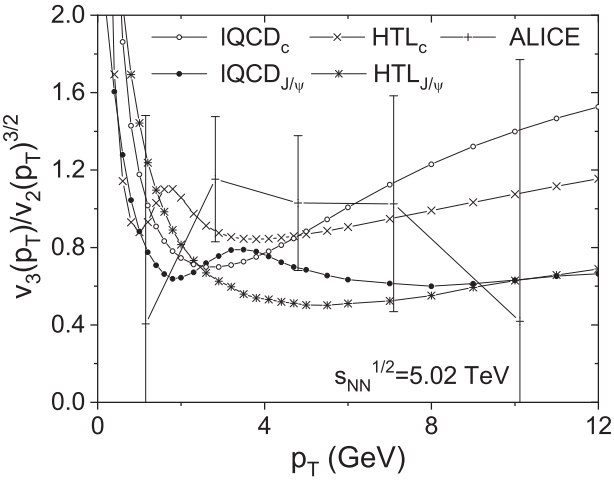

FIG. 10. The plot of the ratio between the elliptic and triangular flow of the J/ψ meson, $v_3/v_2^{3/2}$ at LHC, $\sqrt{s_{\rm NN}} = 5.02$ TeV as a function of transverse momenta, together with the experimental measurement of $v_3/v_2^{3/2}$ by ALICE Collaboration [47] are shown. I also show the plot of the ratio, $v_3/v_2^{3/2}$ between bare charm quark elliptic and triangular flow obtained from the POWLANG transport setup, Fig. 3 in the HTL and lQCD transport coefficients [43] as a function of transverse momenta for comparison.

find $v_{2,J/\psi}^{1/2}(p_T)/v_{3,J/\psi}^{1/3}(p_T)$ varying a little around $2^{1/2}/2^{1/3} \approx 1.12$ in the range between 1.10 and 1.19 inside the medium with the lQCD transport coefficient in the POWLANG. On the other hand, the same ratio increases from 0.9–1.25 and approaches 1.12 as p_T increases due to different behaviors of $v_{2,c}^{1/2}(p_T/2)$ and $v_{3,c}^{1/3}(p_T/2)$ in the medium with the HTL transport coefficient as shown in Fig. 9(b).

The variation of the ratio $v_{2,J/\psi}^{1/2}(p_T)/v_{3,J/\psi}^{1/3}(p_T)$ as a function of transverse momentum presented in Fig. 9(a) and 9(b) implies that the elliptic and triangular flow of charmonium states in the strongly coupled medium, i.e., in the lQCD transport coefficient develops in the same way as functions of transverse momentum, whereas elliptic and triangular flow of charmonium states develops easily in a different way in a weakly coupled medium, i.e., in the HTL transport coefficient in the POWLANG. Therefore, if the medium, the quark-gluon plasma is strongly coupled, the elliptic and the triangular flow of the J/ψ behaves in a similar way, leading to the constant ratio for $v_{2,J/\psi}^{1/2}(p_T)/v_{3,J/\psi}^{1/3}(p_T)$.

In order to investigate in more detail the transverse momentum dependence of the elliptic and triangular flow, I evaluate the ratio $v_3/v_2^{3/2}$ of the J/ψ, which are found to be more sensitive than $v_3^{1/3}/v_2^{1/2}$ [49]. Shown in Fig. 10 is the plot of the above ratio between the elliptic and triangular flow of the J/ψ meson $v_3/v_2^{3/2}$ at LHC, $\sqrt{s_{\rm NN}} = 5.02$ TeV as a function of transverse momentum, together with the experimental measurement of $v_3/v_2^{3/2}$ by ALICE Collaboration [47]. Also shown is the plot of the ratio $v_3/v_2^{3/2}$ between bare charm quark elliptic and triangular flow obtained from the POWLANG transport setup, Fig. 3 in the HTL and lQCD transport coefficients [43] as a function of transverse momentum for comparison.

As the measurement of the ratio $v_3/v_2^{3/2}$ at LHC is made at forward rapidity region of $2.5 < y < 4$ in 0–50 % centralities, direct comparisons between the measurements at LHC and the present results obtained at midrapidity in 20–40% centralities cannot be made. Nevertheless, when the relation between the flow harmonics of the J/ψ and those of charm quarks, i.e., $v_{n,J/\psi}(p_T) \approx 2v_{n,c}(p_T/2)$, holds, the ratio $v_3/v_2^{3/2}$ is expected to be approximately $2/2^{3/2}\, v_{3,c}(p_T/2)/v_{2,c}^{3/2}(p_T/2)$. As shown in Fig. 9 the ratio does not exhibit a constant at low transverse momentum region, but it approaches to $2/2^{3/2} \approx 0.71$ as both the $v_{3,c}(p_T/2)$ and $v_{2,c}^{3/2}(p_T/2)$ converges to equal value due to the same path-length-dependent energy loss with increasing transverse momentum [50].

V. SUMMARY AND CONCLUSION

I have discussed in this paper the elliptic and triangular flow of J/ψ, $\psi(2S)$, and $\chi_c(1P)$ mesons in heavy ion collisions based on the coalescence model. Starting from the evaluation of transverse momentum distributions and yields of those charmonia, I have calculated elliptic and triangular flow of charmonium states when they are produced by charm quark recombination. I have investigated the dependence of not only transverse momentum distributions and yields, but also elliptic and triangular flow of the J/ψ, $\psi(2S)$, and $\chi_c(1P)$ on their internal structures via their wave function distributions in momentum space. I have also discussed further the quark number scaling of elliptic and triangular flow for charmonium states, and have studied in detail the elliptic and triangular flow at low transverse momentum region.

Following the argument that the internal structure, or the wave function difference, is the main factor affecting yields and transverse momentum distributions of different charmonium states, i.e., the J/ψ, $\psi(2S)$, and $\chi_c(1P)$ meson when they are produced from the same number and kind of constituents, a charm and anticharm quark by regeneration at the phase boundary [19], I first investigate in detail the dependence of transverse momentum distributions and yields of the J/ψ, $\psi(2S)$, and $\chi_{c1}(1P)$ meson on their wave function distributions.

I consider three different Wigner functions constructed from the wave function of the J/ψ, $\psi(2S)$, and $\chi_c(1P)$ meson, and calculate the transverse momentum distributions and yields of those charmonium states. The explicit dependence of transverse momentum distributions and yields of charmonium states on their internal structures via their wave function distributions is observed, and as a result, the origin for the possibly large production of the $\psi(2S)$ meson, half as large as that of the J/ψ, is explained.

Using different transverse momentum distributions of the J/ψ, $\psi(2S)$, and $\chi_{c1}(1P)$ meson, I then explore charmonia flow harmonics such as v_2 and v_3 as an attempt to understand possible dependence of the elliptic and triangular flow of charmonium states also on their internal structures via their different transverse momentum distributions.

I adopt here the elliptic and triangular flow of charm quarks obtained by the POWLANG transport analysis, which de-

scribes time evolutions of heavy quarks in heavy ion collisions through the relativistic Langevin equation. I consider two kinds of flow harmonics of charm quarks based on both weak coupling transport coefficients from hard thermal loop (HTL) resummation analysis, and transport coefficients from nonperturbative lattice quantum chromodynamics (QCD) calculation in POWLANG transport setup [43].

The elliptic and triangular flow of J/ψ, $\psi(2S)$, and $\chi_c(1P)$ mesons are found to be only slightly different at both RHIC and LHC energies, irrespective of two cases, flow harmonics of constituent charm quarks considered in two different interactions in the medium, the lQCD and HTL transport coefficients in the POWLANG analysis.

Thereby, further examination on the v_n itself is made, and both the numerator and denominator part of v_n are shown to be actually dependent on the internal structure or the wave function distribution in the momentum space of each charmonium state, whereas the flow harmonics of all charmonium states are evaluated to be almost the same or independent of the internal structure of each charmonium when those are calculated with the wave function distribution dependent numerator and denominator. It can be realized that the similar amounts of contribution to both the numerator and denominator of the v_n from different transverse momentum distributions of charmonium states are canceled out of each other, resulting in almost the same flow harmonics for all charmonium states.

In addition to the v_n, flow harmonics of charmonium states divided by the number of constituents, $v_n/2$ are also studied. The relation similar to the well-known relation between the elliptic flow of mesons and that of constituent quarks can be found for charmonium states, the quark number scaling of flow harmonics; the flow harmonics of charmonium states are approximately twice that of charm quarks $v_{n,c\bar{c}}(p_T) \approx 2v_{n,c}(p_T/2)$.

I then investigate whether the behavior of elliptic and triangular flow at low transverse momentum region $v_n \sim p_T^n$ also holds for charmonium states by focusing those of the J/ψ at LHC energies. For that purpose, the behavior of the $J/\psi\, v_n^{1/n}/p_T$ is examined as a function of transverse momentum, and is also compared to that of bare charm quarks. It can be seen that the $v_n^{1/n}/p_T$ behaves differently at low and intermediate transverse momentum regions, depending on the interaction strengths between charm quarks and the medium. It has been found that the elliptic and triangular flow of charmonium states, the $v_n^{1/n}/p_T$ in the lQCD transport coefficient vary in the similar ways as functions of transverse momentum, whereas those of charmonium states vary easily in different manners in a weakly coupled medium with the HTL transport coefficients.

In relation to the $v_n^{1/n}/p_T$, the transverse momentum dependence of the ratio between the elliptic and triangular flow $v_3^{1/3}/v_2^{1/2}$ as well as $v_3/v_2^{2/3}$ is also studied. It is found that the ratio $v_3/v_2^{3/2}$ is approximately $2/2^{3/2}\, v_{3,c}(p_T/2)/v_{2,c}^{3/2}(p_T/2)$, again simply from the relation $v_{n,c\bar{c}}(p_T) \approx 2v_{n,c}(p_T/2)$, and approaches to $2/2^{3/2} \approx 0.71$ as the transverse momentum increases, and thereby both the $v_{3,c}(p_T/2)$ and $v_{2,c}^{3/2}(p_T/2)$ experiences the same path-length-dependent energy loss, regardless of two different charm quark interactions with the medium, the lQCD and HTL transport coefficients in the POWLANG transport analysis.

Given the relation between the flow harmonics of the J/ψ and those of charm quarks, i.e., $v_{n,J/\psi}(p_T) \approx 2v_{n,c}(p_T/2)$ here, it is natural to observe that the $v_n^{1/n}/p_T$ of the J/ψ cannot be a constant at two times the transverse momentum of the charm quarks unless that of charm quarks is a constant at low transverse momentum regions. By the same token, it seems possible to infer various properties of bare charm quarks inversely from the elliptic or triangular flow of charmonium states as a function of transverse momentum.

Therefore, the question on why the $v_n^{1/n}/p_T$ of charm quarks is a constant, or why the v_n of charm quarks is proportional to p_T^n at low transverse momentum region should be answered before the investigation on $v_n^{1/n}/p_T$ of the J/ψ as a function of transverse momentum is made, which needs further studies in the future. It should be of much worth to extract as much information of charm quarks as possible from charmonium states composed of a charm and an anticharm quarks as properties of charm quarks at the moment of hadronization is not well understood compared to those of light quarks.

As shown previously, the elliptic and triangular flow of charmonium states are all found to be almost identical with very slight differences, and the relation $v_{n,c\bar{c}}(p_T) \approx 2v_{n,c}(p_T/2)$ holds for all charmonium states. Thus, it does not seem easy to understand recent measurements by CMS Collaboration on different elliptic flows for the J/ψ and $\psi(2S)$ [22] entirely from the consideration of different internal structure effects when different charmonium states are regenerated from a charm and an anticharm quarks at the quark hadron phase boundary.

Therefore, in order to explain the measurements by CMS Collaboration, it would be necessary to find other ways to accommodate the effects from different internal structures as well as other different features of charmonium states on not only their flow harmonics but also transverse momentum distributions. Along with the development in theory, I also hope the more precise measurement of the anisotropic flow of the J/ψ and $\psi(2S)$ meson at low transverse momentum regions in the near future will help us to make a clear understanding on the transverse momentum dependence of different charmonia flow harmonics in heavy ion collision experiments.

Considering that the elliptic or triangular flow of charmonium states is one of the important observables directly connected to that of charm quarks by the relation $v_{n,c\bar{c}}(p_T) \approx 2v_{n,c}(p_T/2)$ at low and intermediate transverse momentum regions, I insist that studying the charmonia anisotropic flow provides good opportunities to probe not only flow harmonics but also other properties of charm quarks in heavy ion collisions.

Furthermore, as charmonia production is one of the valuable cases to observe the production of different hadrons with different internal structures but produced from both the same number and kind of constituents, investigating not only the transverse momentum distributions, yields, and anisotropic flow but also other closely relevant observables of the J/ψ, $\psi(2S)$, and $\chi_{c1}(1P)$ meson when they are produced from a

charm and an anticharm quarks by quark coalescence would be helpful in understanding in more detail the hadron production mechanism in heavy ion collisions, finally resulting in the broadening of the understanding on the properties of the QGP.

ACKNOWLEDGMENTS

This work was supported by the National Research Foundation of Korea (NRF) grant funded by the Korea government (MSIT) (No. 2018R1A5A1025563) and (No. RS-2023-00280831).

[1] E. V. Shuryak, Phys. Rep. **61**, 71 (1980).
[2] T. Matsui and H. Satz, Phys. Lett. B **178**, 416 (1986).
[3] P. Braun-Munzinger and J. Stachel, Phys. Lett. B **490**, 196 (2000).
[4] R. L. Thews, M. Schroedter, and J. Rafelski, Phys. Rev. C **63**, 054905 (2001).
[5] A. Andronic, P. Braun-Munzinger, K. Redlich, and J. Stachel, Phys. Lett. B **652**, 259 (2007).
[6] H. Satz, J. Phys. G **32**, R25 (2006).
[7] F. Karsch, D. Kharzeev, and H. Satz, Phys. Lett. B **637**, 75 (2006).
[8] A. Mocsy and P. Petreczky, Phys. Rev. Lett. **99**, 211602 (2007).
[9] A. Adare *et al.* (STAR Collaboration), Phys. Rev. Lett. **98**, 232301 (2007).
[10] B. Abelev *et al.* (ALICE Collaboration), Phys. Rev. Lett. **109**, 072301 (2012).
[11] B. B. Abelev *et al.* (ALICE Collaboration), Phys. Lett. B **734**, 314 (2014).
[12] S. Acharya *et al.* (ALICE Collaboration), Phys. Rev. Lett. **132**, 042301 (2024).
[13] V. Khachatryan *et al.* (CMS Collaboration), Phys. Rev. Lett. **113**, 262301 (2014).
[14] M. Aaboud *et al.* (ATLAS Collaboration), Eur. Phys. J. C **78**, 762 (2018).
[15] V. Greco, C. M. Ko, and P. Levai, Phys. Rev. Lett. **90**, 202302 (2003).
[16] V. Greco, C. M. Ko, and P. Levai, Phys. Rev. C **68**, 034904 (2003).
[17] R. J. Fries, B. Muller, C. Nonaka, and S. A. Bass, Phys. Rev. Lett. **90**, 202303 (2003).
[18] R. J. Fries, B. Muller, C. Nonaka, and S. A. Bass, Phys. Rev. C **68**, 044902 (2003).
[19] S. Cho, Phys. Rev. C **91**, 054914 (2015).
[20] D. Molnar and S. A. Voloshin, Phys. Rev. Lett. **91**, 092301 (2003).
[21] E. Abbas *et al.* (ALICE Collaboration), Phys. Rev. Lett. **111**, 162301 (2013).
[22] A. Tumasyan *et al.* (CMS Collaboration), J. High Energy Phys. 10 (2023) 115.
[23] B. Alver and G. Roland, Phys. Rev. C **81**, 054905 (2010).
[24] B. H. Alver, C. Gombeaud, M. Luzum, and J. Y. Ollitrault, Phys. Rev. C **82**, 034913 (2010).
[25] H. Petersen, G. Y. Qin, S. A. Bass, and B. Muller, Phys. Rev. C **82**, 041901(R) (2010).
[26] M. Nahrgang, J. Aichelin, S. Bass, P. B. Gossiaux, and K. Werner, Phys. Rev. C **91**, 014904 (2015).
[27] M. Singh, M. Kurian, S. Jeon, and C. Gale, Phys. Rev. C **108**, 054901 (2023).
[28] V. Greco, C. M. Ko, and R. Rapp, Phys. Lett. B **595**, 202 (2004).
[29] Y. Oh, C. M. Ko, S. H. Lee, and S. Yasui, Phys. Rev. C **79**, 044905 (2009).
[30] A. J. Baltz and C. Dover, Phys. Rev. C **53**, 362 (1996).
[31] Y. Kanada-En'yo and B. Muller, Phys. Rev. C **74**, 061901(R) (2006).
[32] S. Cho *et al.* (ExHIC Collaboration), Phys. Rev. C **84**, 064910 (2011).
[33] M. Kordell, R. J. Fries, and C. M. Ko, Ann. Phys. (NY) **443**, 168960 (2022).
[34] M. Hillery, R. F. O'Connell, M. O. Scully, and E. P. Wigner, Phys. Rep. **106**, 121 (1984).
[35] R. Scheibl and U. W. Heinz, Phys. Rev. C **59**, 1585 (1999).
[36] S. Cho, K. J. Sun, C. M. Ko, S. H. Lee, and Y. Oh, Phys. Rev. C **101**, 024909 (2020).
[37] S. Cho and S. H. Lee, Phys. Rev. C **101**, 024902 (2020).
[38] S. Plumari, V. Minissale, S. K. Das, G. Coci, and V. Greco, Eur. Phys. J. C **78**, 348 (2018).
[39] S. Cho *et al.* (ExHIC Collaboration), Prog. Part. Nucl. Phys. **95**, 279 (2017).
[40] J. Adam *et al.* (STAR Collaboration), Phys. Lett. B **797**, 134917 (2019).
[41] S. Acharya *et al.* (ALICE Collaboration), Phys. Lett. B **805**, 135434 (2020).
[42] J. Beringer *et al.* (Particle Data Group Collaboration), Phys. Rev. D **86**, 010001 (2012).
[43] A. Beraudo, A. De Pace, M. Monteno, M. Nardi, and F. Prino, J. High Energy Phys. 02 (2018) 043.
[44] M. Luzum and J. Y. Ollitrault, Phys. Rev. C **87**, 044907 (2013).
[45] L. Adamczyk *et al.* (STAR Collaboration), Phys. Rev. Lett. **111**, 052301 (2013).
[46] S. Acharya *et al.* (ALICE Collaboration), Phys. Rev. Lett. **119**, 242301 (2017).
[47] S. Acharya *et al.* (ALICE Collaboration), J. High Energy Phys. 10 (2020) 141.
[48] P. M. Dinh, N. Borghini, and J. Y. Ollitrault, Phys. Lett. B **477**, 51 (2000).
[49] S. Acharya *et al.* (ALICE Collaboration), J. High Energy Phys. 09 (2018) 006.
[50] B. Abelev *et al.* (ALICE Collaboration), Phys. Lett. B **719**, 18 (2013).